Noise Characteristics for Random Fiber Lasers with Rayleigh Distributed Feedback

Bhavaye Saxena

Supervisor: Dr. Xiaoyi Bao
Co-supervisor: Dr. Liang Chen

Thesis submitted to the
Faculty of Graduate and Postdoctoral Studies
in partial fulfilment of the requirements
for the Master's Degree in Physics

Department of Physics
Faculty of Sciences
University of Ottawa

Statement of Originality

This work contains no material which has been accepted for the award of any other degree or diploma in an University or other tertiary institution and, to the best of my knowledge and belief, contains no material previously published or written by another person, except where due reference has been made in the text.

I give consent to this copy of my thesis, when deposited in the University Library, being available for loan and photocopying.

Signed: _____

Date: _____

Supervisors: Dr. Xiaoyi Bao and Dr. Liang Chen

Dedicated to my family

Abstract

Frequency and intensity noise are characterized for Erbium-Doped Fiber and Brillouin random lasers based on Rayleigh distributed feedback mechanism. We propose a theoretical model for the frequency noise of an Er-doped fiber random lasers using the property of random phase modulations from multiple scattering points in ultra-long fibers. We find that the Rayleigh feedback suppresses the noise at higher frequencies by introducing a Lorentzian envelope over the thermal frequency noise of a long fiber cavity. The theoretical model and measured frequency noise agree quantitatively with two fitting parameters. A similar model, which also includes additional acoustic fluctuations and a distributed gain profile in the fiber, has been speculated for the Brillouin random laser. These random laser exhibits a frequency noise level of <6 Hz^2/Hz at 2 kHz, which is lower than what is found in conventional narrow-linewidth EDF fiber lasers and Nonplanar Ring Laser oscillators (NPRO) by a factor of 166 and 2 respectively.

Acknowledgement

I would like to thank my supervisor, Professor Xiaoyi Bao for endowing me this opportunity to have my masters in her group. With her profound knowledge in physics, critical thinking, and her great sense of intuition, she has always been able to provide the best advice in fulfilling my goals regarding this research. Her perseverance and dedication towards this field of research is astounding, and will always be regarded as a source of inspiration. This thesis would be impossible without her constant support and guidance. I would also like to thank Professor Liang Chen, especially for his precious help and countless suggestions regarding the derivations for this thesis. His profound knowledge in physics and mathematics cannot be unmatched, and has always inspired me to challenge all obstacles that come in the way of my research.

I also thank Dr. Pang Meng for helping me understand the phase demodulation scheme for the Frequency Noise measurements, and also for his efforts in helping me build the interferometer. I would also like to thank Dr. Zhonghua Ou for his support in building the Brillouin random laser and doing the necessary measurements for this laser.

I could not imagine what the lab would be like without all my colleagues: Ms. Daisy Williams, Dr. Chams Baker, Mr. Yang Li, Mr. Yang Lu, Mr. Ping Lu, Dr. Xiaozhen Wang, Dr. Dapeng Zhou, Ms. Meiqi Ren, Mr. Dao Xiang and Mr. Hugo Laroque. They have always been there for helpful discussions, and to motivate me at my worst times.

Last, but not the least, I shall sincerely thank my family and friends for all their support and encouragement. Their blessings shall never be forgotten.

Contents

List of Figures

List of Tables

Acronyms

AOM Acousto-Optic Modulator. 44, 45

ASE Amplified Spontaneous Emission. 5, 14, 19, 41

BRFL Brillouin Random Fiber Laser. 20, 38–40, 42, 43, 45, 54, 57–60

EDF Er-doped Fiber. 2–4, 13, 18, 19, 24, 27–29, 31, 32, 34–36, 38, 40, 42, 43, 45, 52, 54–60, 62

EDFA Er-doped Fiber Amplifier. 21

FBG Fiber Bragg Grating. 2, 19, 58

FP Fabry Pérot. 5, 7, 33

ISO Optical Isolator. 19, 21

MZI Mach-Zehnder Interferometer. 43, 44

RIN Relative Intensity Noise. 41, 53, 57, 62

SBS Stimulated Brillouin Scattering. 2, 14, 15, 20

SRS Stimulated Raman Scattering. 15

WDM Wavelength Division Multiplexer. 19

Chapter 1

Introduction

1.1 Motivation

Multiple scattering is a well-known phenomena that occurs in nearly all optical materials. It is therefore quite common and determines the appearance of, for example, clouds, powders, human tissues and even optical materials such as photonic crystals and optical fibers. Hence, it is clear that such defects are difficult to avoid even with the best industrial techniques available, and will always introduce unwanted defects in the stability of conventional optical devices. This perspective on disorder gives birth to a new field of optics which embraces the scattering properties found in all photonics materials to introduce new functionalities in optical systems.

This new approach towards multiple scattering gives rise to what is called a *random laser*. When a highly scattering source is combined with an optical gain media above lasing threshold, these optical cavities force light to propagate in a random walk, similar to the Brownian motion of particles suspended in liquid. However, because these optical wavelets are still highly coherent, they attain a well defined phase, leading to unique interferometric properties that are far more rich and complex than what is achieved by conventional lasers.

Random lasers attain several advantages over regular lasers. Because of the abundance and variety of scattering materials present in the industrial scale, they impose low production costs and simplicity in fabrication. These lasers do not require

extremely customized methods required to create repeatable high-precision micro-cavities. Moreover, with certain modifications, it is feasible to attain performance levels that even challenge conventional lasers. With recent progress in theoretical understanding and experimental advances in random lasing, this new class of lasers show potential in providing more viable solutions for various laser applications, and could even overcome the limitations found in most conventional lasers.

1.2 Statement of Originality

In this thesis, we demonstrate two novel random laser configurations, and characterize their frequency noise for the first time. The first configuration consists of a regular Er-doped Fiber (EDF) for optical gain, a Fiber Bragg Grating (FBG) for wavelength selectivity, and a standard fiber that provides the multiple scattering from the intrinsic Rayleigh scattering. Without compromising its power efficiency and low-noise characteristics, we achieve the most compact Rayleigh scattering random fiber laser to date, using fiber lengths as short as 560m. We also propose a theoretical model for the frequency noise of such random lasers using the property of random phase modulations from multiple scattering points in ultra-long fibers. We find that the Rayleigh feedback suppresses the noise at higher frequencies by introducing a Lorentzian envelope over the thermal frequency noise of a long fiber cavity. The theoretical model and measured frequency noise agree quantitatively with two fitting parameters.

The second configuration utilises the complementary effects of Stimulated Brillouin Scattering (SBS) and Rayleigh scattering distributed across a 10km standard fiber to realise the most compact, single-mode low-noise Brillouin random fiber laser to date. In this case, a bi-directionally pumped tested laser generates the Brillouin gain, while the intrinsic Rayleigh scattering partially traps the light for lasing conditions. Because of the complexity of the distributed gain profile throughout the fiber, a theoretical analysis for the frequency noise has not been calculated explicitly for this laser, but has currently been speculated. Experimental results have also been qualitatively compared with the noise results for the EDF random laser.

In addition to the frequency noise measurements for each laser, preliminary results regarding the power output, power efficiency, laser linewidth, as well as the relative intensity noise have also been conducted to give more insight about the mechanism of each laser.

1.3 Thesis Outline

Chapter 2 begins with introducing the random lasers, explains how they function, and how they can be characterized in terms of their cavity designs. It then provides a historical background on the development of the theoretical understanding and experimental advances for all kinds of random lasers present till date. The chapter then focuses on the different scattering techniques and gain mechanisms found in random fiber lasers, along with a historical background on past contributions specifically regarding these lasers. Finally, with this knowledge, the schematics and lasing mechanisms for the two novel random fiber lasers are presented.

Chapter 3 delves into the frequency noise characteristics for the random lasers in question. Following an introductory section that provides the basic mathematical terminologies of the frequency noise, it discusses the origins as well as derive the expression for thermal frequency noise in regular EDF laser. Then, a novel simplistic model is introduced for the frequency noise in random lasers by taking into account the presence of Rayleigh scattering in the long passive fiber. These calculations provide a simple parametric equation which demonstrates the suppression of the intrinsic thermal frequency noise by the Rayleigh scattering in EDF random laser. Finally, we present some speculations for the frequency noise in Brillouin random fiber lasers.

Chapter 4 begins with demonstrating the preliminary measurement schemes, such as the power output, linewidth, and relative intensity noise that aid in ensuring a single-mode laser emission, as well as approximately determine the magnitude of the frequency noise. This is followed by the schematics for measuring the frequency noise of a given laser using the Phase demodulation method with a 3×3 coupler and the Differential Cross Multiplication Algorithm. This scheme is calibrated using a tested

single-mode narrow-linewidth fiber laser.

Chapter 5 provides a detailed noise characterization for each laser under question. The results for the frequency and intensity noise for the random lasers are thoroughly discussed, and are used to gain more insight of the lasing mechanisms for each laser. The theoretical model for the EDF random laser is validated, and the success and drawback of the current model is also presented. The noise measurements for these random lasers are also compared with those from a variety of conventional narrow-linewidth lasers.

Chapter 6 concludes the thesis, followed by a brief discussion on future work that can be implemented from the knowledge we have attained so far.

Chapter 2

Random Lasers

2.1 What is a Random Laser?

Lasers, in general, rely on two basic elements: a gain medium that provides light amplification through the stimulated emission of photons from an excited atom; and an optical cavity built using waveguides and reflectors that partially confine this light. Initially, in the absence of input photons, the gain medium spontaneously emits light from the excited atoms, providing us with an Amplified Spontaneous Emission (ASE). It is only when part of this emission is reflected back using the optical cavity that amplification through stimulated emission is feasible. Such reflectors are usually not ideal and impose a certain loss in the photon population. When the photon generation rate, or optical gain, exceeds the photon loss rate, we attain a threshold, and the system *lases*. Because of the limited number of excited atoms in the system, the photon population will not be able to increase indefinitely, and the gain is known to saturate. This gain saturation plays a huge role in ensuring a balanced steady-state value for the number of photons in the oscillator.

For a given gain medium, most conventional optical cavity configurations are usually derived from either a Fabry Pérot (FP), or a ring cavity design. The FP cavity (fig. 2.1 a)) consists of two end mirrors placed around the gain medium, allowing the photons to travel through the optical gain in both directions. The ring cavity (fig. 2.1 b)), on the other hand, forces the photons to travel unidirectionally

in a closed loop configuration either using a finite number of reflectors, or a closed loop waveguide (e.g. fiber ring lasers). Because of the fixed cavity length in both configurations, the phase feedback for the photons is fixed, and hence the interference effect imposed on these photons becomes strongly correlated with the spatial profile of the cavity. Such lasers tend to emit a discrete set of equally separated peaks in frequency, where each peak is called a single longitudinal mode, or simply a *mode*.

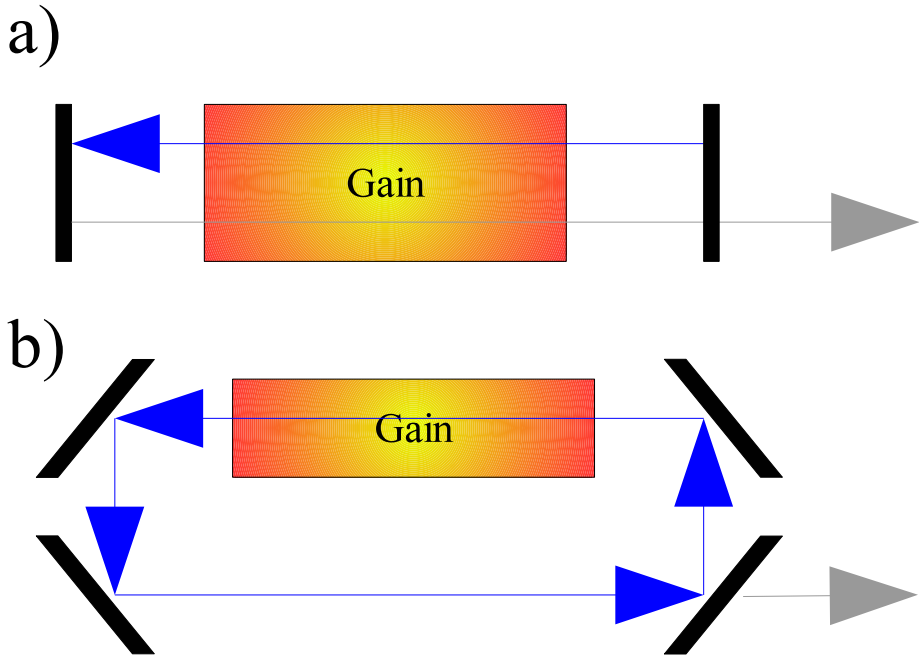

Figure 2.1: Common cavity configurations used in conventional lasers: a) Fabry-Pérot etalon allowing light to travel back and forth; b) Ring cavity design which enforces unidirectionality of light through the gain media.

Random lasers, in contrast to conventional lasers, consist of a randomly scattering disordered media, and hence are sometimes referred to as 'mirror-less' lasers. Usually, the presence of optical scattering in conventional lasers tends to remove some photons from the dominant modes of a conventional cavity, making it a detrimental feature for these lasers. However, it is the same optical scattering that plays a positive role in the amplification and oscillation within such random cavities. Similar to regular lasers, conditions for laser oscillation are favoured only if the net gain exceeds the cavity losses, and the stability depends on the saturation of this gain after threshold. However, the difference in this case is that such lasers consist of a random phase

feedback, which depends on the interference effect induced on each photon as it takes a random walk through the disordered media. Hence, the modes from these lasers tend to be more dense and are randomly separated. Moreover, each mode is introduced to varying gain and loss profiles, resulting in an ensemble of modes with varying coherence properties. Random lasers, even though being 'mirror-less', are definitely not 'mode-less'.

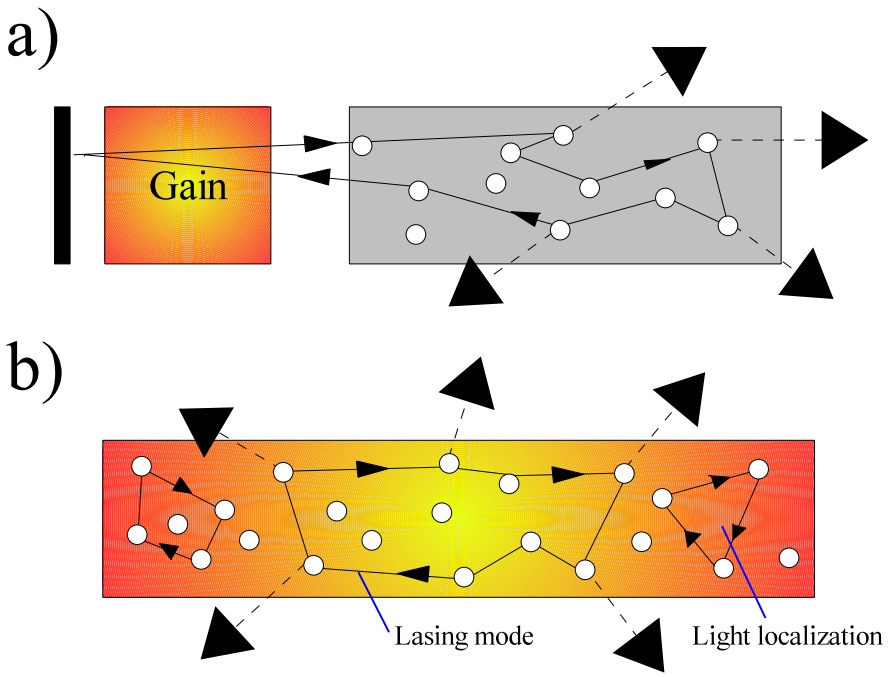

Figure 2.2: Common cavity configurations used in random lasers: a) Modified Fabry-Pérot with a passive scattering medium. A possible lasing mode is shown with the light propagating in a random walk, and partially emitting some of the light in multiple directions b) Disordered gain media with artificial scattering points distributed throughout the fiber. Along with a possible lasing mode, a subset of constructively interfering closed modes due to tightly spaced highly reflecting scattering points can also exist. This process is known as light localization.

Although there are a large variety of materials and techniques used to obtain a random laser, they can essentially be classified into two categories. The first category includes random lasers with passive scattering sources and a regular gain medium. Essentially, these types of lasers are very similar to regular FP lasers, except one of the mirrors is replaced by a random scattering source (figure 2.2 a)). Beyond threshold, only those modes that overcome the varying intrinsic loss imposed by the scatterer

are allowed to resonate. This loss depends on the reflection coefficient of the material, as well as the number of times the light bounces off from each scattering point before reaching the gain medium.

The second category includes random lasers with disordered gain media. In this case, scattering points are present within the gain media itself (figure 2.2 b)). Here, the gain can be distributed more evenly across the spatial profile of the modes, increasing their coherence properties in contrast to the previous category. However, with sufficient number of high scattering points, and surrounded with adequate gain, such lasers can sometimes provide a subset of randomly spaced closed modes that interfere constructively within the medium. This effect is known as *light localization* [2, 3]. Localization only occurs for strong scattering materials, with the added requirement that the mean free path between two scattering points l must be less than the reciprocal of the wavevector k: $kl \leq 1$. This is known as the Ioffe-Regel criterion [3, 4].

2.2 Origins of Random Lasers

Although the term *random lasing* was introduced in 1995 [3], the idea originated during the 1960s, when significant interest in light diffusion with gain was shown by Letokhov and co-workers [5]. Using a diffusive model, it was argued that for an amplified diffusive process, the gain is proportional to the volume, whereas the loss is proportional to the total surface. Hence, at a certain threshold, the intensity should diverge when the gain exceeds the losses in the cavity. Moreover, with wavelength-selective features introduced by the gain, the model also predicted to acquire a narrowing process where the maximum intensity is achieved at a wavelength where the gain is maximum. Taking this model into account, several types of disordered gain media were made by Briskina [6] and Migus [7] using finely ground laser crystals [3], as well as suspending microparticles in laser dyes [8]. As predicted, emission spectra were shown to narrow down with increasing peak intensities. Hence, the random lasers were born.

Although the model by Lekhotov was able to describe the emission properties for the random laser, it neglected a very important aspect. The simplistic diffusion model was not able to take into account the interference effects that are imposed on each photon as it undergoes a random walk through the scattering medium. The need to take this effect in account became clear when several theoretical calculations and experiments related to photon statistics of a random laser indicated that these lasers in fact were behaving similar to regular lasers. Beenakker [9] was able to show that excess photon noise, which originates from the interference between spontaneous and stimulated emission in regular lasers, was also evident for random lasers beyond threshold. Florescu and John calculated the second-order coherence, which measures the fluctuation in intensity, and predicted that above threshold, random lasers exhibit Poissonian statistics that is only evident in coherent lasers [10]. These photon statistics were first observed and confirmed experimentally by Cao [11]. In addition, narrow stochastic spikes were evident over the global narrow emission in random lasers observed by Cao and co-workers [3, 11]. These peaks were later found in all random lasers irrespective of the density and the strength of the scatterers. After significant discussion in the literature, it was clear that all random lasers are definitely bound to be coherent, and that a more thorough model was required to explain the resonant features. Eventually, an alternative mechanism was proposed by Apalkov which stated that certain resonant modes could be formed by chance in the presence of the randomly fluctuating refractive index [12]. These modes, accompanied with sufficient gain, provided a longer lifetime to a specific set of 'lucky photons', which hence gave rise to the observed stochastic spikes. This was experimentally confirmed by Chabanov through the measurement of the decay rate statistics of the modes [13]. A numerical simulation was also calculated by Mujumdar, which emphasized that within a finite-sized random system, there will always be a subset of modes with very long lifetimes in the presence of sufficient gain [14].

At present, there is already a wide range of materials and techniques that can provide enough scattering to realize random lasing. Most common practices for ade-

quate scattering include grinding a material into powder form, suspending scattering elements in a solution, and by etching a porous network of air into the optical media [3]. Depending on the purpose, these materials can either be passive components, which are then complemented by a regular gain material, or they can act as the gain medium themselves. Because of the availability of a variety of scattering materials in the industrial scale, along with the low production cost and simplicity in fabrication, random lasers clearly have an added advantage over regular lasers, which in contrast rely on high-precision methods to create accurate and repeatable cavities. This has sparked significant interest towards random lasers in the laser community, where slowly more emphasis is given towards methods to modify these lasers for application purposes.

Random lasers with high-dimensional optical cavities tend to have poor directionality, require more pump power, and usually consist of a broad emission spectrum. Hence, deriving schemes for a stable operation and beam quality in high-dimensional lasers becomes a very challenging task [15]. However, it has been shown that the complexity of these schemes are reduced significantly with lower-dimension systems. Gottardo was able to control the directionality of the emission in a random laser derived from a anisotropic, birefringent polymer dispersed in liquid crystal, hence mainly emitting plane waves [16]. However, it was later realised that the dimensionality for random lasers can be reduced even further.

2.3 Random Fiber Lasers

Random fiber lasers are one-dimensional lasers that rely on the distributed gain and scattering phenomena derived from silica-based optical fibers. The one-dimensionality arises because of the transverse confinement of light in the presence of a cylindrical fiber waveguide geometry, hence only allowing the cavity to be randomized along the longitudinal direction [**?**]. This provides a great enhancement in the directionality of the output.

Before we can discuss the schematics for these random lasers, we first need to

fully characterize the current scattering and amplification processes that are already available for optical fibers, and how they can contribute towards random lasing.

2.3.1 Random Scattering Processes in Optical Fibers

Rayleigh Scattering

Rayleigh Scattering is known to arise from the interaction of an incident light with the intrinsic dielectric constant fluctuations of given optical fibers [15, 17, 18]. These inhomogeneities can be perceived as a large ensemble of weak reflection points distributed throughout the fiber, providing a backscattered light with a randomised phase feedback. It is considered to be a linear process in the sense that no energy gets transferred between the incident light and silica, and hence no frequency shifts are imposed on the scattering light.

In general, Rayleigh scattering is considered very weak for existing fibers, with a backscattering coefficient as small as $\epsilon = 4.5 \times 10^{-5}$ km^{-1} [15]. However, because of the confinement of light in the cylindrical waveguide, this effect gets accumulated over long fiber lengths. Because Rayleigh scattering occurs in all directions, an intrinsic length-dependent loss is also imposed on the incident light. For light in the 1550 nm window, this Rayleigh loss coefficient is about $0.12 - 0.16$ (dB/km) [19].

Rayleigh scattering only relies on the static density fluctuations spread throughout the fiber, and hence can also be achieved even if the fiber remained unchanged in time. However, temporal perturbations in this scattering arise due to the non-propagating thermal fluctuations present in the media as it exchanges heat energy with the surrounding environment. Hence, this time dependence adds more complexity as well as randomness in the phase feedback acquired from the backscatter.

Strong Scattering points through Etching/Grating

Rayleigh scattering, although useful, cannot be achieved using short fiber lengths. Hence, for compact random lasers, extrinsic modifications to the waveguide need to be implemented for strong scattering properties. There are essentially two approaches

to achieve this task. First, one can inscribe random Bragg gratings along the core of a stardard fiber using intense ultraviolet lasers, resulting in strong scattering points with highly varying refractive indices and phase feedback values. Second, speciality fibers can also be manufactured, giving us freedom to either significantly vary in the core size, etch air gaps within the waveguide, or even doped fibers with strongly scattering particles.

Mode Distribution in Strongly Scattering vs. Rayleigh Scattering Random lasers

The random interferometric properties imposed on light due to the scattering points in the fiber suggest that only some modes will interfere constructively. Strong scattering random lasers consist of a discrete ensemble of scattering point with well defined reflection coefficient and phase feedback (fig. 2.3 a)). Hence, depending on the density of scatterers, the phase-matching conditions for constructive interference are very limited, resulting in a discrete set of resonant modes with random mode separations and varying quality factors. Moreover, in the presence of tightly packed strongly scattering points, it is possible to meet the Ioffe-Regel criteria ($kl \leq 1$), resulting in light localization that can alter the mode structure significantly.

Rayleigh random lasers, on the other hand, cannot attain such a discrete mode distributions mainly due to two factors. First, accumulation of sufficient Rayleigh scattering is only attainable from ultra-long fiber lengths. This significantly increases the number of scatterers in the optical cavity, resulting in an extremely short mean free spectral range between two neighbouring peaks. Second, the presence of temporal perturbations in the fiber density provides randomly varying phase feedback for any given mode, forcing them to drift from their nominal peak, and possibly allow them to overlap with neighbouring peaks. Hence, this large ensemble of densely packed and intrinsically unstable modes can then be perceived as a pseudo-continuous 'modeless' distribution that provides resonance to any wavelength (fig. 2.3 b)). In this case, a combination of a broad gain spectrum and a passive filtration techniques can then

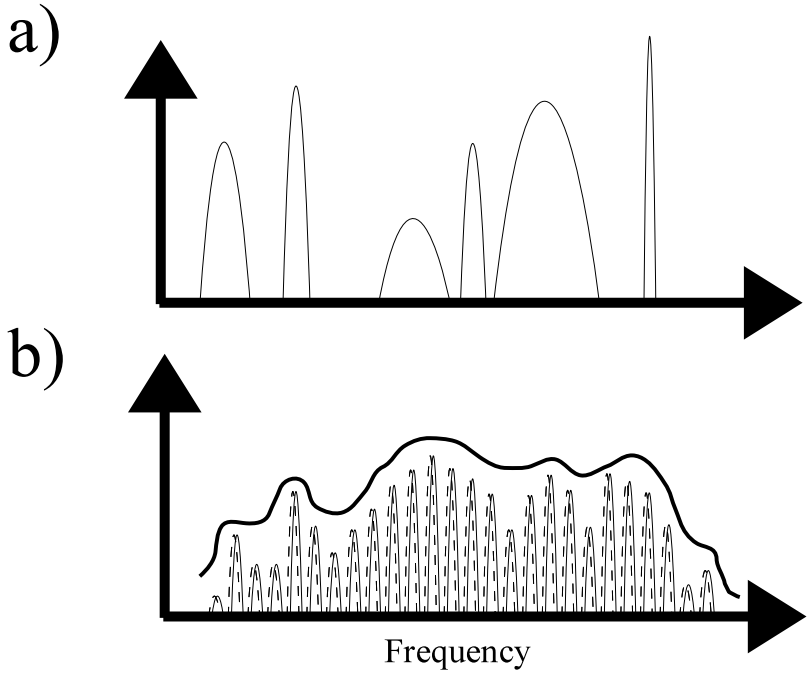

Figure 2.3: Mode Distribution in Strongly Scattering vs. Rayleigh Scattering Random lasers. a) Randomly distributed discrete mode structure in strong scattering random lasers b) Densely packed unstable modes in Rayleigh scattering random lasers, resulting in a overlap of a 'modeless' spectrum

be used to determine lasing conditions for any desired wavelength. The filter aids in suppressing a large number of wavelengths, while the gain provides significant amplification for only those modes with sufficient photon lifetime within the cavity.

2.3.2 Gain Mechanisms in Optical Fibers

Stimulated Emission using Er-doped Fiber (EDF)

The incorporation of trivalent rare-earth ions into silica is a well known process to achieve efficient solid-state lasers and amplifiers. Erbium (Er^{3+}) doped fibers specifically have the added advantage of providing efficient amplification at 1550nm wavelength, which corresponds to the low-loss transmission window in optical fiber communications [20].

Er:glass fibers essentially provides stimulated emission through a quasi-three-level system (fig. 2.4). The pump light, which can either have a wavelength of 980 nm or 1480 nm, excites the Erbium ions into the $^4I_{11/2}$ state for 980 nm pump light

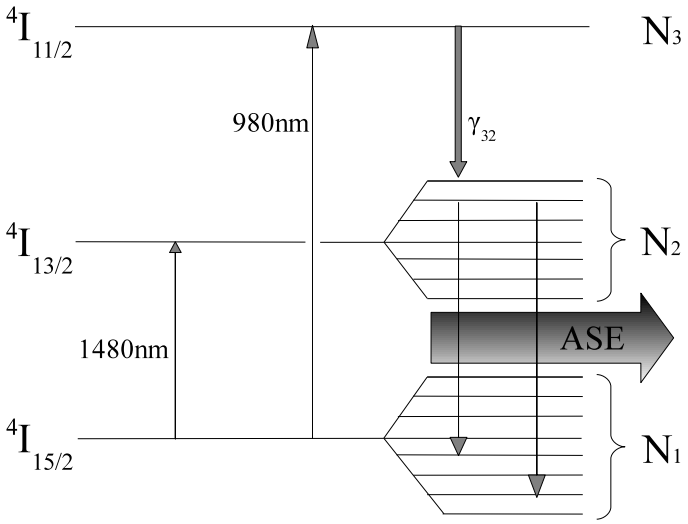

Figure 2.4: Simplified Energy Level Diagram for Er^{3+} [1]

(and $^4I_{13/2}$ for 1480 nm pumped light), after which the 1550nm wavelength region is amplified by stimulated emission, bringing the ions back to the ground state $^4I_{15/2}$. The added Stark splitting, as well as the inhomogeneous broadening effect due to the amorphous nature of glass results in a rather broad ASE, with its peak at 1530nm (this corresponds to the transition from $^4I_{13/2}$ to $^4I_{15/2}$) [1, 20].

With high concentration doping, sufficient amplification can be attained with fiber lengths as short as a few meters. Hence, in random lasers, Er-doped fibers are usually assisted with a passive Rayleigh scattering fiber, or are inscribed with random gratings to produce strong scattering points in the fiber itself.

Gain through Stimulated Brillouin Scattering (SBS)

SBS is the process of a nonlinear interaction between pump and Stokes field through an acoustic wave. A high intensity pump laser produces an acoustic wave through the process of electrostriction [19]. This wave in turn modulates the refractive index as it travels through the medium. Hence, the pump light begins to scatter from the acoustic wave. Because of the Doppler effect, the scattered light is down-shifted to the

Stokes frequency. Eventually, a mutual interaction between the acoustic and Stokes waves is enforced, and both their amplitudes are allowed to grow [21]. Through the conservation of energy and momentum, the frequencies ω_p and ω_s and wave vectors $\mathbf{k}_p$ and $\mathbf{k}_s$ of the pump and Stokes wave respectively are related by [21]:

$$\Omega_B = \omega_p - \omega_s \tag{2.1}$$

$$\mathbf{k}_A = \mathbf{k}_p - \mathbf{k}_s \tag{2.2}$$

where Ω_B and $\mathbf{k}_A$ are the frequency and wave vector of the acoustic wave respectively. For silica fibers, the Brillouin down-shift is found to be $\sim$ 10GHz away from the nominal pump frequency [19].

The gain for the Stokes wave is generally very narrow ($\sim$10 MHz), as it relates to the damping time of the acoustic waves, and is known to have a Lorentzian shape [19]. This gain through SBS can be used to amplify weak signals with a frequency equal to that of the Stokes wave. Naturally, the signal is injected from the opposite direction of the pump signal.

The two main advantages of using Brillouin gain is that: first, it is an intrinsic gain mechanism derived from a standard optical fiber; and second, the gain is distributed throughout the long fiber. This means that one can easily generate a Brillouin random laser using just a standard optical fiber and a tested pump laser. With the combined effects of Rayleigh scattering, the optical fiber itself behaves as a disordered gain medium.

Gain through Stimulated Raman Scattering (SRS)

Similar to Brillouin scattering, Stimulated Raman Scattering (SRS) is the process of the nonlinear interaction between the pump and Stokes wave through the excitation of vibrational modes in a given medium. According to the Raman effect, it is possible for a molecule to absorb a pump photon of frequency ω_p, but scatter back a photon with Stokes frequency ω_s as it changes to one of the vibrational states, and not back

to the initial state [19]. For an intense pump field, this nonlinear interaction gets amplified significantly and a large amount of the pump energy gets transferred to the Stoke wave.

In contrast to Brillouin gain, Raman gain usually extends to ∼40 THz lower than pump frequency, with the peak width around ∼10 THz [19]. This occurs due to the amorphous nature of silica, which provides a broad and almost continuous band of molecular vibrational states.

Raman gain shares the same advantages as mentioned in Brillouin gain, and can also be applied for random lasing when combined with Rayleigh scattering in ultra-long fibers. However, there are two main drawbacks: first, the threshold for Raman gain is extremely high when compared to Brillouin; second: fiber lengths to induce significant Raman gain can exceed 20 km, and can even reach 100 km, making them impractical for application purposes.

2.3.3 Origins of Random Fiber Lasers

The first random fiber laser was introduced by Turitsyn in 2010 [15]. Lasing was achieved from stimulated Raman amplification and Rayleigh scattering present in an 83 km fiber. It was the first time ever when a random laser demonstrated a stationary Gaussian beam with a narrow emission spectrum, along with an efficiency and performance that was comparable to regular lasers. These exciting results opened a whole new field of research that combined the diverse areas of laser physics, disordered systems, fiber optics and non-linear optics. Soon, this laser was followed by a series of modified fiber systems that incorporated already existing fabrication schemes and filtration techniques to search for a vast variety of applications. Some of them include attaining a dual wavelength random laser with Raman gain and a 200 km fiber [22], a low-threshold random fiber laser including a Fiber Bragg Grating [23], a tunable random fiber laser [24], and a random laser with cascaded second-order Raman stokes wavelength [25] along with a low threshold second-order random lasing with Fiber Bragg Gratings. [26].

With the advent of Raman random fiber lasers, alternative random fiber lasers using different gain mechanisms also began to emerge in the fiber optics community. The two most common gain mechanisms include stimulated emission from an Erbium-doped fiber, as well as the amplification of the Stokes waves in Stimulated Brillouin Scattering. Brillouin random lasers were first conceived by Meng, where the Stokes gain was provided by a 25 km fiber in a ring configuration, and the scattering was provided by an additional 10km Rayleigh fiber attached to the ring structure. Frequency stabilization techniques, as well as noise measurements were also presented [27, 28]. For the case of Er-doped fiber random lasers, random scattering feedback was induced by two dominant methods. The first method included fabrication of unique long Fiber Bragg Gratings with some artificially induced randomness on existing Er-doped fibers. This included a single-mode random laser with randomly spaced gratings [29] as well as a 3mW threshold laser with randomly distributed phase error which induce light localization [30]. On the other hand, another approach was taken where a regular Er-doped fiber was spliced alongside an ultra-long passive optical fiber that provides sufficient Rayleigh feedback for random lasing. These fiber systems differed from Raman lasers in the sense that the gain profile was not distributed throughout the fiber, but was only confined within a small portion of the whole fiber length, while the rest of the fiber only contributed to random phase feedback from Rayleigh Scattering. This was first realised by Tao Zhu using a ring cavity consisting of an Er-doped fiber, a tunable filter, and an specially designed 5.7km non-uniform fiber with a high scattering coefficient [31]. An attempt to demonstrate random lasing with the same ring cavity and a Rayleigh scattering 600 m standard fiber was shown in [32]. However, insufficient Er-doped fiber gain and Rayleigh scattering led to a hybrid random laser which also included partial contributions from a regular ring cavity [32].

Several improvements in Er-doped fiber and Brillouin lasers are evident when compared to Raman random lasers: the threshold is greatly reduced by a factor of 100; the fiber lengths used in these laser is reduced by at most a factor of 10; and each of these lasers are able to attain narrow-linewidth ($\sim$1 kHz range) continuous

wave emission, along with additional tuning capabilities that are independent of the cavity length [27,28,31,32]. Such results make them possible alternatives to standard narrow-linewidth lasers for a wide range of applications in optical precision metrology, high-resolution spectroscopy, sensors and communication systems.

With this review, we are now ready to discuss the schematics and lasing mechanisms for two novel single-mode, low noise random fiber lasers.

2.4 Linear Cavity Er-doped Random Fiber Laser

2.4.1 Optimization of Er-doped Fiber Gain

The backscattering coefficient from Rayleigh scattering in fibers is $\epsilon = 4.5 \times 10^{-5}$ $km^{-1} \approx$ -40dB km^{-1}. On the other hand, gain by stimulated emission in Er-doped fibers varies non-linearly with respect to both the pump power and input signal power. This is mainly due to gain saturation effects, and the finite concentration of dopants. Hence, before placing the gain fiber into our laser, it is necessary to measure the gain profile for a given EDF as a function of the variable 980nm pump power and 1550nm input signal power (fig. 2.5).

We realise that even with a high dopant concentration, the gain is not sufficient to overcome the Rayleigh loss. Spontaneous emission levels for EDF in the 1550 nm range are about -25 dBm. This means that the maximum gain that can be achieved in a single pass cannot exceed $\sim$30 dB, while the reflection coefficient from a 1km is lower than -40 dB. Hence, it impossible to achieve random lasing for fiber lengths less than 1 km, and clearly demonstrates the drawback of the ring cavity random laser designs used in [32] and [33]. However, this problem is easily overcome if we take advantage of the additional gain provide by the fiber when placed in a linear cavity. Following the same example, an additional gain of $\sim$10 dB is attained by this technique. Hence, with proper tuning, lasing threshold can now be attained for much shorter lengths of Rayleigh Scattering fibers. We now discuss the schematics regarding the fabrication of such lasers.

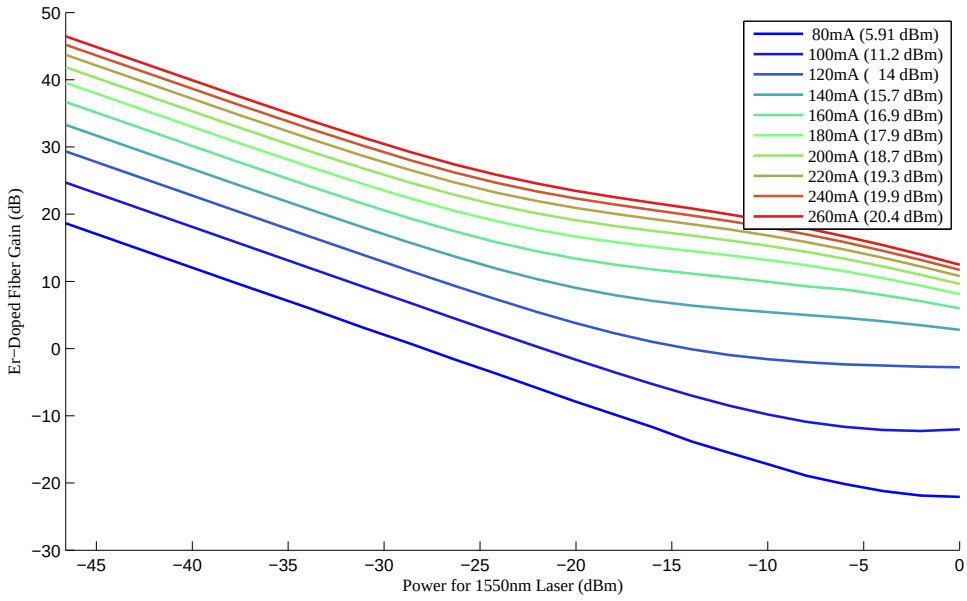

Figure 2.5: Gain profile for 1.3 m LIEKKI^{TM} Er80-8/125 Er-doped fiber with respect to 1550 nm laser power. Legend indicates the pump current (and pump power) injected in each case

2.4.2 Laser Schematics

The laser design for our random laser is shown in figure 2.6. The 1.3 m LIEKKI^{TM} Er80-8/125 EDF is pumped by a FITEL^{TM} 980 nm semiconductor laser through a 980/1550 nm Wavelength Division Multiplexer (WDM). The FBG is used to reflect a narrow wavelength band with a center wavelength of 1539.4 nm and 3 dB bandwidth of 0.03nm from the broad ASE of the EDF. An Optical Isolator (ISO) is used at the output of the laser to eliminate back reflections from external elements by imposing a loss of about 50 dB for any light that travels opposite to the desired direction of propagation. This way, the only source of light travelling back into the cavity, as desired, will be the Rayleigh feedback from the long fiber. With sufficient length for the Rayleigh Scattering Fiber, the accumulated distributed feedback can be large enough to compensate for the loss induced by the half-open cavity configuration of the laser.

No optical fiber connectors are included in this laser. This is to ensure that we do not introduce any unnecessary high reflection points in our cavity that could dominate over the scattering light from the Rayleigh fiber. Moreover, because the connectors

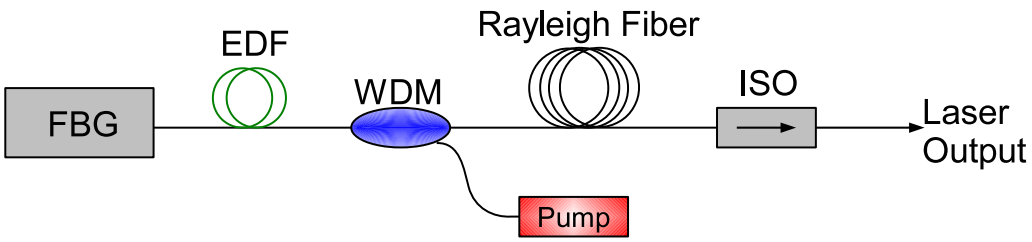

Figure 2.6: Schematics of the EDF random laser. FBG: Fiber Bragg Grating (1539.4 nm). EDF: Erbium Doped Fiber (1.3 m). WDM: Wavelength Division Multiplexer (1550 nm/980 nm). RSF: Rayleigh-Scattering Fiber. ISO: Isolator. Pump laser wavelength: 980 nm

are not permanent, and may include air gaps, these connector might accumulate dust particles over time, hence reducing the reflectivity from the Rayleigh fiber. To overcome such problems, all components are fusion spliced before operation.

2.5 Bi-directionally Pumped Brillouin Random Fiber Laser

2.5.1 Lasing Mechanism

The Brillouin Random Fiber Laser (BRFL) exploits the mutual effect of Rayleigh scattering and Brillouin scattering from a bi-directional pump to obtain a disordered gain media from an ultra-long optical fiber. The lasing mechanism can be explained through a simple model as shown in figure 2.7. As the pump signals is injected from both directions, each signal gives rise to separate acoustic waves that propagate towards each other, while the corresponding Stokes wave travel in the outward direction. Ideally, the Stokes waves should simply leave the fiber unaffected. However, with sufficient fiber lengths, the Rayleigh scattering from the Stokes wave gets accumulated, and acts as the weak input signal for the gain provided by SBS from the counter-propagating pump signal. These amplified Stokes signals once again take part in Rayleigh scattering, and the whole process is repeated.

A more thorough understanding of this laser can be determined by a complex theoretical model developed from the non-linear Maxwell equations for counter-propagating

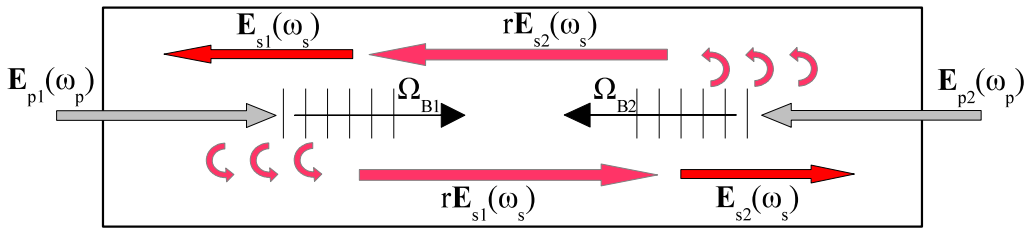

Figure 2.7: Lasing Mechanism for BRFL. Each Stokes wave $\mathbf{E}_{si}$ is scattered back into the fiber, and becomes the seed for SBS gain provided by the acoustic gratings with frequency Ω_j. This amplified field is then superposed with $\mathbf{E}_{sj}$, creating a cyclic loop.

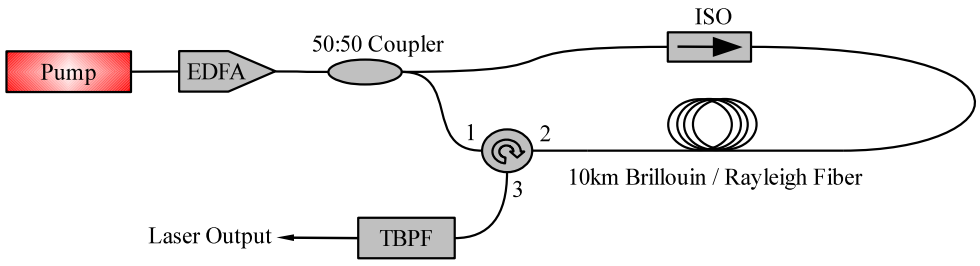

Figure 2.8: Schematics for the BRFL. EDFA: Er-doped Fiber Amplifier. TBPF: Tunable Band-Pass Filter (set at Stokes frequency).

pump and Stokes wave, coupled with the differential equation for the dynamics of two counter-propagating acoustic gratings. Moreover, the Maxwell equations also need to take into account the additional Rayleigh scattering Stokes waves that are vital for lasing conditions. Because of the complexity, analytical or numerical results for this system have not been obtained to date, and is currently under investigation.

2.5.2 Laser Schematics

Ironically, in contrast to such a complex lasing mechanism, the design for such lasers is extremely simple (figure 2.8). We use a tested single mode fiber laser (wavelength is 1550 nm) as the pump laser which is amplified by an Er-doped Fiber Amplifier (EDFA). This pump signal is then equally divided by a $50:50$ optical coupler, and is then launched into a 10 km standard optical fiber through an optical circulator and ISO, respectively, to provide the bi-directional pumping mechanism. The isolator

is used to eliminate back reflections from external elements and ensures that light is only allowed to travel one way by imposing a loss of about 50 dB for any light that travelling in opposite directions. The circulator behaves in a similar fashion, except that the backscattering light is forced to travel through a separate port, and hence provides the output for the laser. A tunable band-pass filter is set to resonate with the Stokes frequency, and deplete any contributions from the pump signal. All components are fusion spliced to ensure no strong scattering points distorted with the desired random lasing mechanism.

Chapter 3

Frequency Noise in Fiber Lasers

Prior to the Rayleigh random fiber lasers mentioned in the previous chapter, not much emphasis was given to the noise characteristics for random lasers. Because these lasers rely on the random multiple scattering from an inhomogeneous optical reflector, a large number of modes are allowed to resonate, resulting in a random ensemble of narrow spikes over the emission spectrum of the laser [3]. This also meant that these lasers intrinsically lacked any filtration scheme to select an individual mode. Hence, any noise characteristics (linewidth, frequency noise, relative intensity noise) that are used to characterize single-mode resonators, cannot be applied for such unstable multi-mode resonators. However, the recent developments of single-mode Rayleigh random fiber lasers as shown in the last chapter brings this new genre of lasers on par with existing narrow-linewidth lasers, and hence allows us to analytically determine their noise characteristics for the first time.

Frequency Noise measurements provide a statistical representation of how far a resonator is likely to deviate from its nominal frequency. Although all lasers will be limited by the spontaneous emission (known as the Schawlow-Townes limit), most lasers cannot reach this level due to the perturbations in the cavity as it interacts with the environment. In the case of waveguides such as fibers, these pertubations arise because of the local strains and changes in the refractive index over time. Hence, in a way, frequency noise measurements play a vital role in understanding the benefits and limitation for a given cavity design. Moreover, analytical results of the frequency

noise become critical in the development of narrow-linewidth lasers.

This chapter demonstrates a novel approach in analytically characterizing the frequency noise of the EDF random laser. It also shows that the Rayleigh feedback from the ultra-long fiber plays a huge role in suppressing the intrinsic noise present in EDF lasers. The first section focuses on the theory of frequency noise, and introduces several mathematical terminologies that will be used in proceeding sections and chapters. The second section will focus on the main contributing factors for frequency noise in EDF lasers, with several analytical equations derived from previous work. The third section will introduce a novel simplistic model to derive the suppressed frequency noise in EDF random lasers, and also compare it with previous analytical results. Finally, we present some speculations for the frequency noise in Brillouin random fiber lasers.

3.1 Theory and Definitions

Assume there is an ideal signal oscillating as a purely sinusoidal wave with a single frequency ν_0, such that:

$$E(t) = E_o sin(2\pi\nu_0 t) \tag{3.1}$$

However, it is known by experience that such pure oscillations are extremely hard to achieve. This is due to the existence of random phase fluctuations that will vary with respect to time [34, 35]. Hence, this will disrupt the single-frequency characteristics of the oscillating signal.

With the introduction of these random phase instabilities, equation (3.1) is modified as follows:

$$E(t) = E_o sin(\Phi(t)) \Rightarrow E_o sin(2\pi\nu_0 t + \phi(t)) \tag{3.2}$$

where $\phi(t)$ represents the phase variations of the wave.

Now, suppose we differentiate $\Phi(t)$ with respect to time (also, we divide this term by 2π):

$$\frac{1}{2\pi}\frac{\mathrm{d}\Phi(t)}{\mathrm{d}t} = \nu_0 + \frac{1}{2\pi}\frac{\mathrm{d}\phi(t)}{\mathrm{d}t} \Rightarrow \nu_0 + \Delta\nu \tag{3.3}$$

Equation (3.3) represents the instantaneous frequency of the signal. As we can see, this includes the sum of two components: 1) the constant frequency ν_0 corresponding to the nominal frequency of the signal; 2) the instantaneous frequency deviation $\Delta\nu$ from the nominal frequency which will vary with respect to time [35]. This fluctuation is considered to be a random wave, i.e. at any time, the waveform can only be known statistically. In this case, it is assumed to be a stationary (meaning that the probability density is time-invariant), zero-mean random variable. With these properties in mind, we can characterize the statistics by the temporal autocorrelation of the variable. The autocorrelation of $\Delta\nu(t)$ is represented as follows [20, 34, 36–38] (assuming $\Delta\nu(t) \in \mathbb{R}$):

$$C_f(\tau) = \langle \Delta\nu(t)\Delta\nu(t+\tau)\rangle = \int_{-\infty}^{\infty} \Delta\nu(t)\Delta\nu(t+\tau)\,\mathrm{d}t. \tag{3.4}$$

Another common way of characterizing the statistics is by taking the Fourier transform of the autocorrelation, which we define as the **Frequency Noise** (with units Hz^2/Hz) of the oscillator, and is represented as follows [20, 34, 36–38]:

$$S_\nu(f) = \mathcal{F}[C_f(\tau)](f) \Rightarrow \mathcal{F}[\langle \Delta\nu(t)\Delta\nu(t+\tau)\rangle](f) \tag{3.5}$$

$$\Rightarrow \mathcal{F}[\Delta\nu(t)]\overline{\mathcal{F}}[\Delta\nu(t)] \Rightarrow |\mathcal{F}[\Delta\nu(t)]|^2(f) \tag{3.6}$$

where $\mathcal{F}[\Delta\nu(t)]$ is the Fourier Transform of the noise wave in the time domain, and $|z|$ is the absolute value of a complex entity. Equation 3.6 can be derived using the Wiener-Khinchin Theorem [20, 37]. The Frequency Noise $S_\nu(f)$ physically corresponds to the mean-square frequency deviations per unit Hz bandwidth centered at the fluctuation frequency f [38].

There are other implications worth mentioning once the frequency noise is obtained. Using this noise, one can obtain the mean-square frequency deviation $\langle \Delta\nu^2 \rangle$, as well as the root-mean square frequency deviation $\Delta\nu_{rms}$ using the following equations [38]:

$$\begin{aligned} \langle \Delta\nu^2 \rangle = C_f(0) &= \left[\int_{-\infty}^{\infty} S_\nu(f) e^{i2\pi f\tau} \, \mathrm{d}f \right]_{\tau=0} \\ \Rightarrow \int_{-\infty}^{\infty} S_\nu(f) \, \mathrm{d}f &= \int_0^{\infty} 2S_\nu(f) \, \mathrm{d}f \end{aligned} \tag{3.7}$$

and

$$\Delta\nu_{rms} = \sqrt{\langle \Delta\nu^2 \rangle} = \left[\int_0^{\infty} 2S_\nu(f) \, \mathrm{d}f \right]^{1/2} \tag{3.8}$$

The conversion from a double-sided integral to a one-sided integral is feasible due to the symmetry of $S_\nu(f)$. However, this conversion has significance while working in the laboratory as most spectrum analysers do not provide a double sided spectrum $S_\nu(f)$, but usually give a single sided spectrum $2S_\nu(f)$ [38]. Lastly, according to [38], the quantity $\Delta\nu_{rms}$ in equation 3.8 is considered a "natural measure of the spectral purity of the laser line" and is closely related to the linewidth of the laser.

3.2 Origins of Frequency Noise in an Er-doped Fiber Lasers Laser

Here, we concern ourselves with the fundamental frequency noise contributions in Er-doped fiber lasers cavity lasers. Note that these noise factors don't include thermal variations, acoustic vibrations, or pump noise that significantly shift the nominal frequency of the laser. Presence of these noise elements will usually amount to low-frequency noise components that are measurable even in the simplest of apparatus, and can be eliminated to a large degree by placing the laser within a controlled environment.

3.2.1 Schawlow-Townes Limit

One of the main conditions mentioned in [39] for lasers to operate is that the number of atoms in the upper level should exceed the number at the lower level. If a photon is travelling through this inverted population medium at a frequency equivalent to the energy difference of the two levels, then it will grow coherently due to the properties of the stimulated emission. However, this light is affected by the spontaneous emission noise that will radiate at that particular frequency, giving rise to random fluctuations in the phase difference between the amplified and the spontaneous emission. This has two main consequences. First, it gives rise to a finite Lorentizian linewidth for the laser oscillation that cannot be eliminated. Second, the signal to noise ratio becomes limited because of the intermingling between the amplified and the spontaneous emission. The reader should note that these are in fact fundamental limits imposed upon all lasers, and cannot be eliminated by any means.

The frequency noise spectral density for the Schawlow-Townes noise limit is described as follows [40, 41]:

$$S_{v-sp}(f) = (1 + \alpha_l^2) n_{sp} \frac{h {\upsilon_l}^3}{Q^2 P} \tag{3.9}$$

where α_l is the linewidth enhancement factor (a proportionality constant which relates the intensity fluctuations with phase fluctuations in the resonator), n_{sp} is the normalized inversion, h is the Planck's constant, υ_l is the laser frequency, Q is the quality factor and P is the laser power. The factors of interest in this equation are Q and P, as we realise that the best way to reduce the frequency noise is to work under high power and high Q-value conditions. Another interesting property of this noise is that the noise spectrum is constant with respect to frequency.

3.2.2 Thermal Noise Limit in Er-doped Fiber Lasers

As mentioned before, perturbations in the laser cavity leads to a noise limit which is significantly higher than the Schawlow-Townes limit. In the case of EDF lasers,

the effective cavity length is known to modulate due the equilibrium temperature fluctuations within the host fiber, resulting in what is known as the *thermal noise* [41, 42]. Several measurements shown by [38, 41, 42] indicate that this noise seems to have a persistent $1/f$ characteristic in the low-frequency range of the frequency noise spectral density, resulting in a residual linewidth. Moreover, it has been shown to be independent of the pump power, and has no correlations with any "technical" noise sources like pump noise or acoustic vibrations [42]. We will now explain in detail the origins of the characteristic $1/f$ thermal frequency noise in Er-doped fiber lasers using the following derivation.

Derivation for thermal noise in EDF lasers

Temperature fluctuations $\Delta T(t, \mathbf{r})$ result in local strain and refractive index changes within a given fiber. Because of this, the local frequency deviation $\dot{\phi}(t, \mathbf{r})$ for a monochromatic light of frequency ω_l passing through the point $\mathbf{r}$ and time t can be written as [43]:

$$\begin{aligned}\dot{\phi}(t, \mathbf{r}) &= -\omega_l \left(\frac{\mathrm{d}\epsilon}{\mathrm{d}T} + \frac{1}{n}\frac{\mathrm{d}n}{\mathrm{d}T} \right) \Delta T(t, \mathbf{r}) \\ &= -\omega_l q \Delta T(t, \mathbf{r}) \end{aligned} \tag{3.10}$$

where q encompasses the strain (ϵ) and refractive index (n) coefficients into a single variable known as the *thermo-optic coefficient*, a intrinsic property of the silica fiber. Using equations 3.4 and 3.6, we can show that the autocorrelation function for the frequency deviation is linearly proportional to the autocorrelation of the thermal fluctuations:

$$\langle \dot{\phi}(\omega, \mathbf{r}) \dot{\phi}(\omega', \mathbf{r}') \rangle = \omega_l^2 q^2 \langle \Delta T(\omega, \mathbf{r}) \Delta T(\omega', \mathbf{r}') \rangle \tag{3.11}$$

In order to calculate the autocorrelation of the thermal fluctuations for an fiber in

thermal equilibrium, we consider the following inhomogeneous heat diffusion equation [42, 43]:

$$c_\nu \Delta\dot{T}(t, \mathbf{r}) - \kappa_t \nabla^2 \Delta T(t, \mathbf{r}) = -\nabla \cdot \mathbf{h} + f \tag{3.12}$$

where c_ν denotes the specific heat at constant volume, κ_t denotes the thermal conductivity, $\mathbf{h}$ corresponds to the random heat current and f corresponds to the rate of heat production per unit volume within the material. At this point, we need to make a clear distinction between the two source terms. Physically, the first term in the right hand side of equation 3.12 represents the thermal fluctuations from an equilibrium state caused by random exchanges of energy between neighbouring elements (heat flow). Hence, this noise is bound to be present in all active and passive components of the laser cavity. However, the second term represents an additional heat energy created from *within* the fiber. This secondary noise source exists due to the heat generated during the spontaneous emission of excited ions in the doped fiber, which in this case represents the pumped EDF [42]. In contrast to the equilibrium thermal noise, this noise is only found in the active components of the cavity. As it will be shown later, it is this noise source that brings rise to the characteristic $1/f$ thermal noise in laser media.

Taking a Fourier transform of equation 3.12 gives us:

$$\Delta T(\omega, \mathbf{k}) = \frac{-i\mathbf{k} \cdot \mathbf{h}(\omega, \mathbf{k}) + f(\omega, \mathbf{k})}{\kappa_t(k^2 + 2ik_1^2)} \tag{3.13}$$

where ω and $\mathbf{k}$ are the Fourier frequency and wave vectors, and $k_1 = \sqrt{\omega c_\nu/(2\kappa_t)}$. Now, we assume that the two source terms $\mathbf{h}$ and f are uncorrelated in space and time such that [42]:

$$\langle h_i(\omega, \mathbf{k}) h_j(\omega', \mathbf{k}') \rangle = 2\kappa_t K T^2 \delta_{ij} \delta(\omega - \omega') \delta^3(\mathbf{k} - \mathbf{k}') \tag{3.14}$$

$$\langle f(\omega, \mathbf{k}) f(\omega', \mathbf{k}') \rangle = Q \delta(\omega - \omega') \delta^3(\mathbf{k} - \mathbf{k}') \tag{3.15}$$

where K is the Boltzmann constant, and Q is an unknown heat constant. We also assume that $\mathbf{h}$ and f are uncorrelated with each other. Hence, from equation 3.13 we get [42]:

$$\langle \Delta T(\omega, \mathbf{k}) \Delta T^*(\omega', \mathbf{k}') \rangle = \frac{(2\kappa_t K T^2 k^2 + Q) \delta(\omega - \omega') \delta^3(\mathbf{k} - \mathbf{k}')}{\kappa_t^2 (k^2 + 2ik_1^2)(k'^2 - 2ik_1'^2)} \tag{3.16}$$

Evaluating the inverse Fourier transform with respect to wave vectors $\mathbf{k}$ and $\mathbf{k}'$ yields the following spatial correlation function [42]:

$$\langle \Delta T(\omega, \mathbf{r}) \Delta T^*(\omega', \mathbf{r}') \rangle = \frac{\delta(\omega - \omega')}{\kappa_t^2} \left(2\kappa_t K T^2 \frac{e^{-k_1 R} \cos(k_1 R)}{R} + \frac{Q}{2k_1^2} \frac{e^{-k_1 R} \sin(k_1 R)}{R} \right) \tag{3.17}$$

where $R = |\mathbf{r} - \mathbf{r}'|$. Already, we can see a $1/f$ divergence in the low frequency limit from the $1/k_1^2$ factor in the second term of equation 3.17. So far, the calculations have been independent of the spatial geometry of the waveguide. Hence, in order to calculate the effective thermal fluctuations in optical fiber, the quantity $\Delta T(\omega, \mathbf{r})$ needs to be averaged over the entire optical mode volume. With a more detailed integration conducted in [43], as well as using equation 3.10, it can be shown that for a fiber cavity length L and a Gaussian mode field radius a, the net frequency noise can be written as [42, 43]:

$$S_\omega(\omega) = S_{eq}(L,\omega) + S_{neq}(L,\omega) \tag{3.18}$$

$$S_{eq}(L,\omega) = \frac{\omega_l^2 q^2 L^{-1} K T^2}{4\kappa_t} \mathrm{Re}\left[e^{ik_1^2 a^2/2} \mathrm{E}_1(ik_1^2 a^2/2)\right] \tag{3.19}$$

$$S_{neq}(L,\omega) = -\frac{\omega_l^2 q^2 L^{-1} Q}{8\kappa_t^2 k_1^2} \mathrm{Im}\left[e^{ik_1^2 a^2/2} \mathrm{E}_1(ik_1^2 a^2/2)\right] \tag{3.20}$$

$$\tag{3.21}$$

where S_{eq} and S_{neq} represents the *equilibrium thermal noise* arising from the random heat current $\mathbf{h}$ and the *non-equilibrium thermal noise* arising from the addition heat source f respectively. $\mathrm{E}_1(z)$ is the standard exponential integration function [42, 43]:

$$\mathrm{E}_1(z) = \int_z^\infty \frac{e^{-t}}{t} \mathrm{d}t \tag{3.22}$$

Note that in equation 3.21, we assumed that the entire cavity consists of an active fiber of length L, resulting in a parametric noise spectrum that only varies according to the source strength Q present in S_{neq}. However, most fiber lasers comprise of a composite cavity consisting of both an EDF and a passive fiber. Since S_{neq} arises from the EDF only, the net thermal frequency noise can be altered as follows:

$$S_\omega(\omega) = S_{eq}(L_{eq} + L_{neq}, \omega) + S_{neq}(L_{neq}, \omega) \tag{3.23}$$

where L_{eq} and L_{neq} are the lengths of the passive and active fiber respectively.

A generic trend for the thermal frequency noise S_ω along with the individual terms S_{eq} and S_{neq} has been shown in figure 3.1. We can clearly see S_{neq} diverging with a $1/f$ noise in the lower frequency limit, while the contributions from S_{eq} tend to saturate. At higher frequencies, both S_{eq} and S_ω roll off with a $1/f^2$ dependence [42].

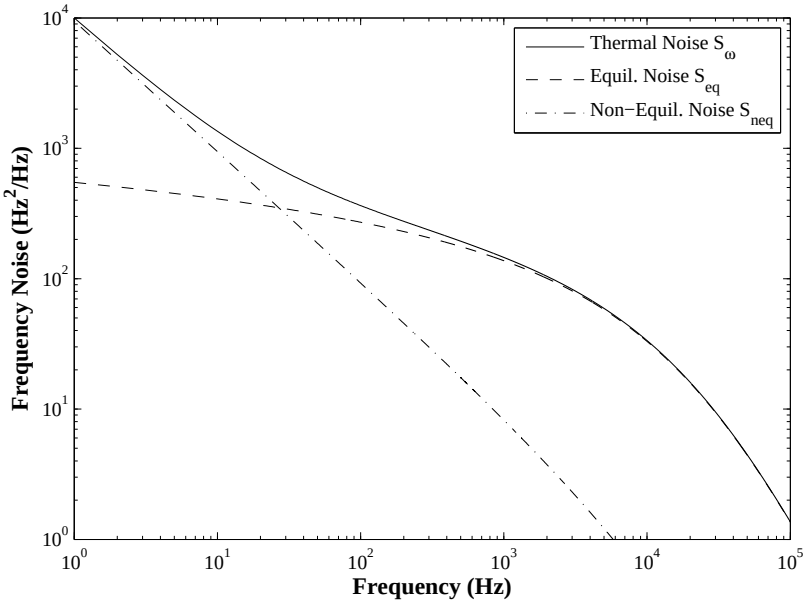

Figure 3.1: Example of Thermal frequency noise in Er-doped Fiber lasers S_ω, along with the individual equilibrium and non-equilbrium noise components S_{eq} and S_{neq} respectively

Hence, we have shown that it is the contribution of the additional random heat source generated from the active EDF that gives rise to the persistent $1/f$ thermal noise spectrum in such fiber lasers. From equation 3.17, we realize that the $1/f$ profile is evident irrespective of the spatial geometry of the fiber, and varies only with respect to the length of the fiber L_{neq}, and the intrinsic source strength Q. It has been shown that Q only depends on the intrinsic properties of the gain media, such as dopant concentration, gain, absorption and mean lifetime of the excited state [42]. A more thorough analysis of the origins of Q goes beyond the scope of this thesis, and can be found in [42].

We now have a strong understanding of the frequency noise characteristics for conventional fiber cavity lasers. In the next section, however, we will modify the existing model to determines the frequency noise for EDF random lasers. This new model will consider the interferometric effect arising from randomly distributed scattering points in a long fiber, resulting in additional noise characteristics that are shown to suppress the intrinsic thermal frequency noise in fibers.

3.3 Frequency Noise Model for Er-doped Fiber Random Lasers

Consider the following ideal scenario as shown in figure 3.2. The first laser (fig. 3.2.a) is a regular Fabry Pérot cavity with two distinct reflectors at either ends and a gain medium. The random laser (fig. 3.2.b) , on the other hand, has a finite ensemble of randomly distributed scattering points, each with different reflecting amplitudes and phase values.

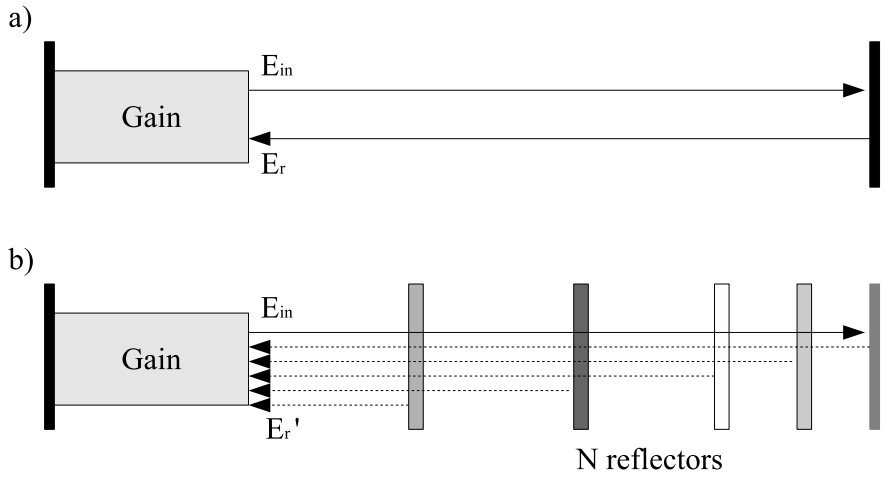

Figure 3.2: Comparison of the reflected field: a) E_r in a Fabry Pérot cavity, b) E'_r in a random laser with N reflectors

We are interested in determining an expression for the reflected field E_r and E'_r for the Fabry Pérot cavity and the random cavity respectively. Assume that each cavity already attains single-mode lasing conditions, and a monochromatic field E_i with a nominal frequency ω_l is emitted by the gain medium. Then the reflected fields E_r and E'_r can be simply written as:

$$E_r(t) = E_i(t)e^{i\phi(t-\tau_1)} \tag{3.24}$$

$$E'_r(t) = E_i(t)\sum_{j=1}^{N} R_j e^{i\phi(t-\tau_j)} \tag{3.25}$$

where τ_j is the finite delay, R_j is the reflection coefficient and $\phi(t-\tau_j)$ is the delayed

phase shift from the j_{th} reflection point. It is evident that all noise characteristics for the FP cavity can be determined from the delayed phase perturbations contributed by the single reflector. Hence, the frequency noise for the FP laser can be written as:

$$S_{FP}(\omega) = \mathcal{F}\left[\langle\dot{\phi}(t-\tau_1)\dot{\phi}(t-\tau_1+\tau)\rangle\right] \tag{3.26}$$

In the case of the random laser, however, the noise characteristics cannot be determined in a straightforward manner. The net phase shift has to constitute of all the phase terms $\phi(t-\tau_j)$ contributed by the ensemble of N reflectors. Assuming the phase perturbations from each reflector to be small, we can apply first order approximations to the exponential in equation 3.25, giving us the following expression:

$$E_r'(t) = E_i(t)M\left(1 + i\Phi(t)\right) \tag{3.27}$$

$$M = \sum_{j=1}^{N} R_j \tag{3.28}$$

$$\Phi(t) = \frac{\sum_{j=1}^{N} R_j\phi(t-\tau_j)}{\sum_{j=1}^{N} R_j} \tag{3.29}$$

Hence, for small phase perturbations, we can claim the net phase shift $\Phi(t)$ for the random laser to be a statistical average of all the phase shift terms $\phi(t-\tau_j)$, where each term is weighted by the normalized reflectivity R_j/M. In this case, the frequency noise for the random laser is:

$$\begin{aligned} S_{Random}(\omega) &= \mathcal{F}\left[\langle\dot{\Phi}(t)\dot{\Phi}(t+\tau)\rangle\right] \\ &= \frac{\sum_{j=1}^{N}\sum_{k=1}^{N} R_jR_k\mathcal{F}\left[\langle\dot{\phi}(t-\tau_j)\dot{\phi}(t-\tau_k+\tau)\rangle\right]}{\sum_{j=1}^{N} R_j\sum_{k=1}^{N} R_k} \end{aligned} \tag{3.30}$$

Using this simplistic model, we can now derive the frequency noise for an EDF random laser with ultra-long Rayleigh feedback fiber.

3.3.1 Derivations for Thermal Frequency Noise in Er-doped Fiber Random Lasers

The derivation is based on the following assumptions:

- Rayleigh scattering in single-mode fibers arises from local inhomogeneities in the refractive index throughout the fiber. These inhomogeneities act as a set of randomly distributed weak reflectors [44]. However, for analytical results, we assume that the fiber only contains uniformly distributed scattering points. The variation in the reflectivity or phase shift from each scattering point is considered negligible.

- The fiber has a mean intrinsic attenuation coefficient α and refractive index n. The speed of light inside the medium is $\nu = c/n$.

- For a given fiber length L, we assume there are N finite scattering points each equally separated by a distance $\nu\delta_\tau$, where δ_τ is the time delay between two segments. Hence, N is inversely proportional to δ_τ as follows:

$$L = N\nu\delta_\tau \tag{3.31}$$

- The length of the EDF is negligibly small compared to the ultra-long Rayleigh scattering passive fiber. According to equation 3.23, this means that $L_{eq} \gg L_{neq}$, which suggests that the $1/f$ contribution from the EDF is going to dominate significantly over the equilibrium thermal noise ($S_{neq} \gg S_{eq}$).

Hence, using equation 3.25, for an incident monochromatic field E_i, the reflected field E_r from a random laser with Rayleigh feedback is represented as:

$$E_r'(t) = \sqrt{R}E_{in}(t) \times \sum_{j=1}^{N} e^{-j\alpha\nu\delta_\tau} \times e^{i\phi(t-j\delta_\tau)} \tag{3.32}$$

Where R is the reflection coefficient for the intensity of the field. Applying first order approximation on $e^{i\phi(t-m\delta_\tau)}$:

$$E'_r(t) = \sqrt{R}E_{in}(t) \times \sum_{j=1}^{N} e^{-j\alpha\nu\delta_\tau} \times (1 + i\phi(t - j\delta_\tau)) \tag{3.33}$$

$$= E_{in} \times M \times (1 + i\Phi_{net}(t)) \tag{3.34}$$

where

$$M = \sqrt{R}\sum_{j=1}^{N} e^{-j\alpha\nu\delta_\tau} \tag{3.35}$$

$$\Phi_{net}(t) = \frac{\sum_{j=1}^{N} e^{-j\alpha\nu\delta_\tau} \times \phi(t - j\delta_\tau)}{\sum_{j=1}^{N} e^{-j\alpha\nu\delta_\tau}} \tag{3.36}$$

Using equation 3.31, the frequency noise for the random laser can be expressed as:

$$S_{\dot{\Phi}_{net}(t)} = \frac{\sum_{j=1}^{N}\sum_{k=1}^{N} e^{-j\alpha\nu\delta_\tau}e^{-k\alpha\nu\delta_\tau}\mathcal{F}\left[\langle\dot{\phi}(t - j\delta_\tau)\dot{\phi}(t - k\delta_\tau + \tau)\rangle\right]}{\sum_{j=1}^{N} e^{-j\alpha\nu\delta_\tau}\sum_{k=1}^{N} e^{-k\alpha\nu\delta_\tau}} \tag{3.37}$$

Using Weiner-Khintchine theorem [20, 37], and the time-shifting property of the Fourier transform:

$$\begin{aligned}\mathcal{F}\left[\langle\dot{\phi}(t - j\delta_\tau)\dot{\phi}(t - k\delta_\tau + \tau)\rangle\right](\omega) &= \mathcal{F}\left[\dot{\phi}(t - j\delta_\tau)\right]\mathcal{F}^*\left[\dot{\phi}(t - k\delta_\tau)\right] \\ &= e^{i(j-k)\omega\delta_\tau}|\dot{\phi}(\omega)|^2 \\ &= e^{i(j-k)\omega\delta_\tau}S_\omega(\omega)\end{aligned} \tag{3.38}$$

Where $S_\omega(\omega)$ represents the thermal frequency for a conventional EDF laser. This simplifies $S_{\dot{\Phi}_{net}(t)}$ into:

$$
\begin{aligned}
S_{\dot{\Phi}_{net}(t)} &= \frac{\sum_{j=1}^{N}\sum_{k=1}^{N} e^{-j\alpha\nu\delta_\tau} e^{-k\alpha\nu\delta_\tau} e^{i(j-k)\omega\delta_\tau}}{\sum_{j=1}^{N} e^{-j\alpha\nu\delta_\tau}\sum_{k=1}^{N} e^{-k\alpha\nu\delta_\tau}} S_\omega(\omega) \\
&= \frac{\sum_{j=1}^{N} e^{-j\alpha\nu\delta_\tau} e^{ij\omega\delta_\tau}}{\sum_{k=1}^{N} e^{-k\alpha\nu\delta_\tau}} \frac{\sum_{k=1}^{N} e^{-k\alpha\nu\delta_\tau} e^{-ik\omega\delta_\tau}}{\sum_{j=1}^{N} e^{-j\alpha\nu\delta_\tau}} S_\omega(\omega) \\
&= \left|\frac{\sum_{j=1}^{N} e^{-j\alpha\nu\delta_\tau} e^{ij\omega\delta_\tau}}{\sum_{k=1}^{N} e^{-k\alpha\nu\delta_\tau}}\right|^2 S_\omega(\omega) \\
&= \left|\frac{1-e^{-(N+1)\alpha\nu\delta_\tau} e^{i(N+1)\omega\delta_\tau}}{1-e^{-\alpha\nu\delta_\tau} e^{i\omega\delta_\tau}} \frac{1-e^{-\alpha\nu\delta_\tau}}{1-e^{-(N+1)\alpha\nu\delta_\tau}}\right|^2 S_\omega(\omega)
\end{aligned}
\tag{3.39}
$$

For ultra-long fiber lasers, we can assume that $L = N\nu\delta_\tau \gg 1m$. Similarly, we can also assume such long fibers to have significantly large number of scattering points, which implies that $N \gg 1$. This simplifies $S_{\dot{\Phi}_{net}(t)}$ even further to:

$$
S_{\dot{\Phi}_{net}(t)} \approx \frac{(\alpha\nu)^2}{(\alpha\nu)^2 + \omega^2} S_\omega(\omega) \tag{3.40}
$$

Hence, we realise for ultra-long fiber random lasers, with sufficiently large number of evenly distributed scattering points, the intrinsic thermal frequency noise present in silica fibers gets suppressed by a Lorentzian envelope. Moreover, the linewidth of this Lorentzian envelope only depends on the intrinsic mean attenuation and refractive index of the fiber. Finally, if we assume $S_\omega(\omega)$ to be a $1/f$ noise in the low frequency limit, the noise for our Er-doped random laser can be parametrically written as [44]:

$$
S_{Random}(\omega) = \frac{(\alpha\nu)^2}{(\alpha\nu)^2 + \omega^2} \frac{A}{\omega} + B \tag{3.41}
$$

where A and B are fitting parameters used to match our theoretical model with experimental results. Since S_{eq} increases as we shorten the fiber length, the value of A varies accordingly. B is assumed to be the background noise that arises from our apparatus, which limits the signal to noise ratio for our measurements. The effect of the Lorentzian envelope over the existing thermal frequency noise in the high

frequency range is clearly shown in figure 3.3.

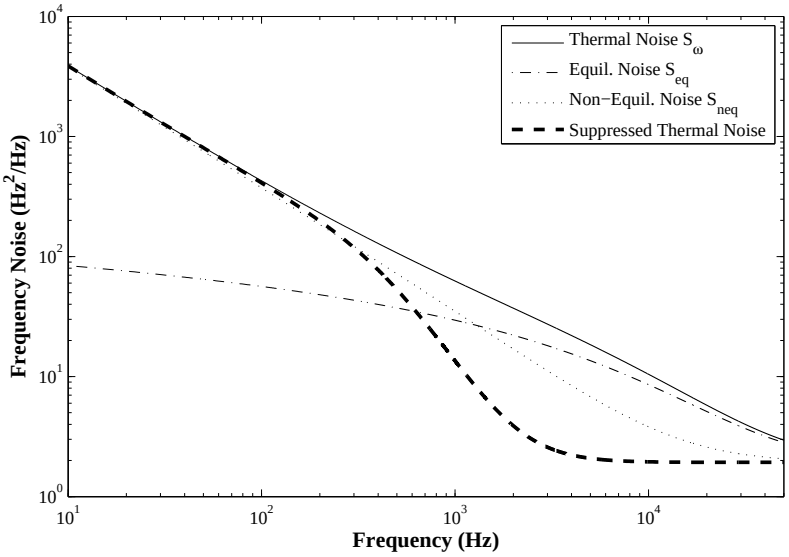

Figure 3.3: Suppression of high frequency-range thermal frequency noise by a Lorentzian envelope in EDF random laser with ultra-long Rayleigh feedback. Parametric values from eq. 3.41: $A = 4\times10^4$ Hz^2; $B = 2$ Hz^2/Hz; Linewidth for Lorentzian envelope $\alpha\nu/2\pi = 870$ Hz

This derivation for the frequency noise of the random laser was inspired from past contributions by Yoshino [45] and Nakagawa [46]. Comparison between our theoretical model and experimental are shown in chapter 5.

3.4 Frequency Noise in Brillouin Random Fiber Lasers

As mentioned in section 2.5, the steady state solutions for the amplified Stokes and acoustic waves for a bi-directionally pumped optical fiber have not been determined to date, and are currently under investigation. However, this does not stop us from speculating the contributing factors for the frequency noise in the BRFL, and how it could possibly differ from the noise contribution in the EDF random laser as mentioned previously. The two proposed contributing factors are as follows:

3.4.1 Pressure Fluctuations in Brillouin fiber lasers

According to Boyd [21], changes in the dielectric constant $\Delta\epsilon$ in the fiber (for a given temperature T) are linearly proportional to the density fluctuations $\Delta\rho$ as follows:

$$\Delta\epsilon = \left(\frac{\delta\epsilon}{\delta\rho}\right)_T \Delta\rho \tag{3.42}$$

This density fluctuation can be further expressed as a function of two more thermodynamic variables, such as pressure p and temperature T:

$$\Delta\rho = \left(\frac{\delta\rho}{\delta p}\right)_T \Delta p + \left(\frac{\delta\rho}{\delta T}\right)_p \Delta T \tag{3.43}$$

The second term in this equation has already been shown to contribute to the thermal frequency noise in fiber lasers (section 3.2.2). These fluctuations are governed by the inhomogeneous diffusion equation (eq. 3.12) which consists of the two noise sources $\nabla \cdot \mathbf{h}$ and $\mathbf{f}$. For the BRFL, we can assume no heat source is present ($\mathbf{f} = 0$), and the thermal noise is only contributed from the random heat current $\mathbf{h}$.

However, in this case, the first term indicates that pressure fluctuations will also contribute to the frequency noise of the laser. We predict that due to the electrostriction present in the fiber, an additional random pressure source will superpose over the existing resonant pressure waves (or acoustic waves) as they propagate through the medium. Interactions between this acoustic wave and the pump would hence lead to additional phase fluctuations in the Stokes wave.

Unlike in the previous case, the dynamics for this acoustic fluctuations will now be governed by the following equations of motion:

$$\Delta\ddot{p}(t,\mathbf{r}) - \Gamma'\Delta\dot{p}(t,\mathbf{r}) - \nu^2\nabla^2 p(t,\mathbf{r}) = \mathbf{g} \tag{3.44}$$

where $\mathbf{g}$ represents the additional pressure source present due to electrostriction.

Using this equation, one can apply similar techniques as in section 3.2.2 to obtain the autocorrelation for $\Delta p(t, \mathbf{r})$, and hence, derive the frequency noise in Brillouin fiber lasers due to acoustic fluctuations.

3.4.2 Distributed Gain Characteristics in Brillouin Random Fiber Lasers

The pressure fluctuations mentioned above are predicted to occur in both regular Brillouin fiber lasers and BRFLs. However, the interferometric properties due to Rayleigh scattering found only in BRFLs will impose additional characteristics that may or may not aid in suppression of the frequency noise. For the case of EDF random lasers, we assumed most of the fiber was passive, and hence only acquire an intrinsic attenuation coefficient α. However, depending on the steady state solutions for bi-directional pumped BRFLs, it is possible that the gain will be distributed throughout the fiber unevenly. Hence, the reflected field from incident monochromatic field E_{in} cannot be written as in equation 3.25, and needs to be generalised as follows:

$$E_r'(t) = \sqrt{R}E_{in}(t) \times \sum_{j=1}^{N} G_z(j\nu\delta_\tau) \times e^{i\phi(t-j\delta_\tau)} \tag{3.45}$$

where $G_z(z)$ represent the average gain (or attenuation) that is acquired by the field as it is reflected from a point z along the fiber. At this point, since not much is known about the distributed gain profile, one cannot possibly predict the kind of envelope that is formed in order to suppress the intrinsic acoustic and thermal noise features in BRFLs (unlike the explicit Lorentzian envelope derived in the case for thermal noise).

We have now fully characterized the frequency noise characteristics for EDF random lasers, and speculated the contributing factors for the frequency noise in the BRFLs. Hence, we can now divert our attention towards the methodology applied to acquire the intensity and frequency noise measurements for these random lasers.

Chapter 4

Methodology

The methodology to characterize the noise for any given laser mainly consists of three stages. First, it is necessary to determine whether the emission from the given system is in fact a laser. This requires us to measure three essential variables: lasing threshold power, power efficiency, and the linewidth. The first two variables can be determined by measuring the laser output power with respect to varying pump power. The linewidth, on the other hand, is determined from the Self-Heterodyne Method using a Mach-Zehnder interferometer. Failure to achieve any of these results will indicate that system is only emitting an incoherent ASE.

After verifying these preliminary results, more sophisticated methods can be implemented to provide an in-depth analysis on the coherent properties of a given system. In this case, the correlations between two measurements for the instantaneous frequency, or the frequency noise, is measured using the 3×3 coupler based Phase Demodulation Method, followed by the Differential-Cross-Multiplication Algorithm for signal processing. In addition, the Relative Intensity Noise (RIN) is also measured to determine the correlation between two intensity (or amplitude) values measured at different times.

4.1 Preliminary Measurements and Results

4.1.1 Lasing threshold and Power efficiency

The lasing threshold is the power level which determines a sudden change in the slope of the output power of the laser with respect to the pump power. At this point, the gain present in the laser begins the exceed the loss imposed by the optical cavity. The slope of the output power beyond this point represent the power efficiency of the laser, and represents the net gain provided by the lasing system.

In our case, we measured the laser output for three lasers: two EDF random lasers, one with a 1km standard Rayleigh scattering fiber, and another with a 10km fiber; one BRFL with a 10km standard fiber. The design for each random laser have already been discussed in sections 2.4 and 2.5. Variation of the laser output power with respect to the pump power were measured using a Thorlabs^{TM} PM100D power meter.

The results are shown in figure 4.1. In the case of EDF random lasers, threshold for the 1 km fiber laser is obtained at 75 mW with a power efficiency of $\sim$0.15, while the threshold for the 10 km fiber is at 62 mW with a power efficiency of $\sim$0.1. However, there is a slight drop in the power efficiency for the 10 km case beyond 100 mW pump power. This suggests that the laser has attained a threshold for other nonlinear effects inside the Rayleigh fiber, which will be explained later on in chapter 5. Note that no lasing threshold is attained in the absence of a Rayleigh fiber in the random laser. The only power that is measured comes from the background ASE noise of the Er-doped fiber. This shows that no strong reflecting sources are present, and the cavity is only dependent on the scattering from the Rayleigh fiber. For the 10km BRFL, the lasing threshold is obtained at $\sim$22 mW with a power efficiency of only 0.04. This low threshold level indicates that the Brillouin gain in the BRFL is far much higher than what is provided by the EDF for the same length in the fiber. However, it seems that the BRFL suffers from external power loss arising from other passive components, such as the optical coupler and the band-pass filter, resulting in

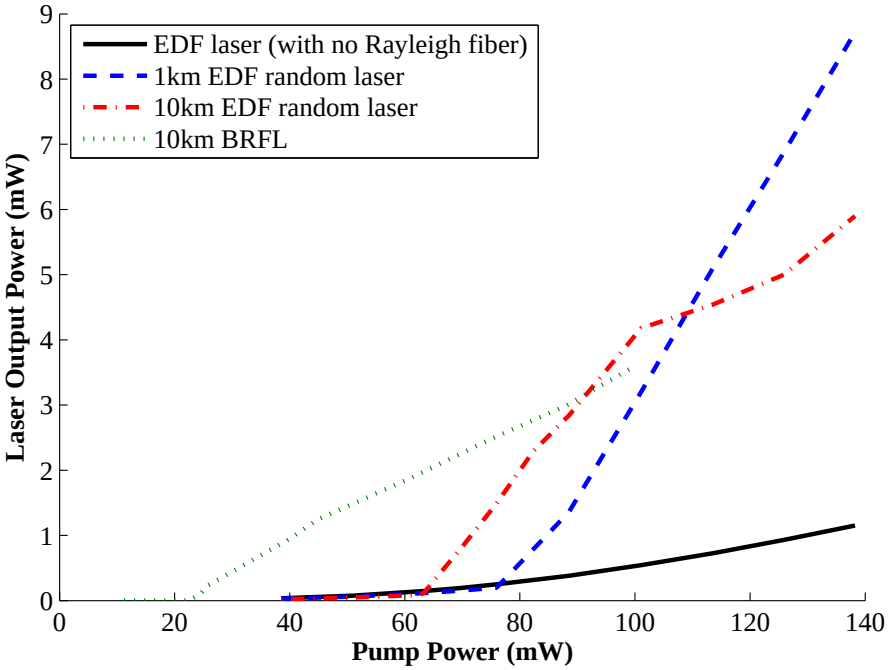

Figure 4.1: Laser output power vs pump power for random lasers with variable Rayleigh fiber lengths. SMF: single-mode fiber

a much lower power efficiency than what is predicted from a high gain BRFL.

Two general characteristics regarding random lasers can be obtained from these measurements. First, an increase in the Rayleigh fiber length results in a higher accumulation of power from the multiple scattering, leading to a lower threshold power. Second, for a fixed gain, the net attenuation accumulated by the output light increases as it passes through a longer Rayleigh fiber, resulting in a lower power efficiency. Out of all the lasers mentioned, it seems that the 1 km EDF random laser provides the best power efficiency for an adequately high threshold power.

4.1.2 Self-Heterodyne Method for Linewidth measurements

Linewidth measurements for fiber lasers are conducted using a Mach-Zehnder Interferometer (MZI) as shown in 4.2. In this case, the path difference must exceed the coherence length, hence allowing the laser field to interfere incoherently with a delayed version of itself. Through this technique, one is able to translate the spectral density of the laser's frequency noise from the optical domain to the radio frequency

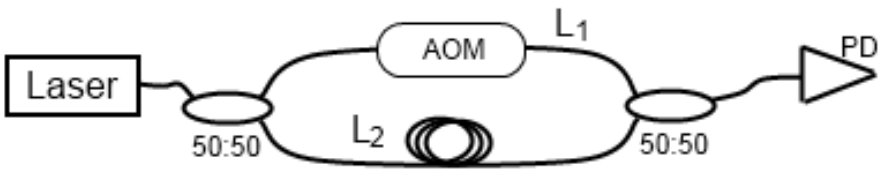

Figure 4.2: Experimental setup for Self Heterodyne Method. Each coupler has a 50:50 coupling ratio. PD: photodetector; AOM: Acousto-Optic Modulator

domain, making it ideal for signal processing.

In order to derive the linewidth, we assume the frequency noise for a monochromatic field $E(t)$ is only influenced by the Schawlow-Townes limit, implying that the frequency noise $S_\nu(f)$ is flat. From this, the laser field spectrum $S_E(f)$ can be derived to be a Lorentzian centred at the nominal frequency f_0 [39, 47, 48]:

$$S_E(\omega) = E_0^2 \frac{\gamma/\pi}{\gamma^2 + (\omega - \omega_0)^2} \tag{4.1}$$

where γ represents the *linewidth* of the laser. When this field $E(t)$ is subjected to the Self-Heterodyne apparatus (fig 4.2), we can express the generalized laser field at the detector as follows [39, 48, 49]:

$$E_T(t) = \frac{1}{4} E_0 e^{i\omega_0 t} [e^{i\phi(t)} + e^{i[\Omega t + \omega_0 t_d + \phi(t+t_d)]}] \tag{4.2}$$

Here, t_d is the time delay induced by the path difference $L2 - L1$ in the MZI. The Acousto-Optic Modulator (AOM) downshifts the frequency of the signal in one of the arms by Ω. With rigorous calculations for the current i_d detected from the photo-diode, and applying the condition $t_d \to \infty$ to represent incoherence between the two arms, the spectrum of the photo-current in the frequency domain results to [39, 48, 49]:

Table 4.1: Linewidth for EDF Random Lasers and BRFL

Laser	Linewidth (kHz)	Coherence length (km)
1km EDF random laser	3.23	61.9
10km EDF random laser	5.21	38.4
10km BRFL	2.33	90.1

$$S_{i_d}(\omega) = \frac{2S^2E_0^4}{\pi}[4\delta(\omega) + \frac{2\gamma}{(2\gamma)^2 + (\omega - \Omega)^2}] \tag{4.3}$$

where this time, the linewidth for $S_{i_d}(f)$ is simply twice of what is obtained in $S_E(f)$ [39, 48, 49]. This clear relation between the two spectrum is exploited to determine the true linewidth for a monochromatic field subject to the Schawlow-Townes limit.

The Self-Heterodyne method was applied using a Mach-Zehnder interferometer with a path difference of 100km. The AOM downshifts the incoming frequency by 40 MHz. An Agilent Electrical Spectrum Analyser was used to obtain the one sided spectrum. A Lorentzian fitting was applied to the acquired data. The linewidth results for the 1 km and 10 km EDF random lasers, as well as the 10km BRFL are shown in table 4.1.

It is to be noted that none of these calculations take into account the intrusion of the $1/f$ characteristics of the frequency noise for an arbitrary laser, and assume a laser only bears the Schawlow-Townes limit. It has been shown in [49, 50] that the inclusion of the $1/f$ frequency noise combined with the flat frequency noise leads to a Voigt lineshape. However, even these modifications still falls under the assumption that the thermal noise exactly bears a $1/f$ characteristics. This may be true for a semiconductor laser [41], but may not be as accurate for a fiber laser, as seen in [38, 41, 42].

The significance of using the Self-Heterodyne method is to approximately determine the linewidth of the laser, through which we can determine the coherence length

of the laser. This knowledge of the coherence length will become vital as we move towards a more sophisticated schematic to determine the noise characteristics for any arbitrary laser.

4.2 Frequency Noise Measurement using Phase Demodulation Method based on a 3×3 coupler.

Fiber Interferometers tend to have a very high sensitivity, and hence have been used as a sensing apparatus inside various devices, such as hydrophones, accelerometers and spectrophones [51, 52]. The output intensity from the interferometers usually has a cosine relationship with the phase variations, however, demodulating this signal with high accuracy and resolution is not straightforward [52]. The output usually suffers from thermal-drift induced signal fading, leading to changes in the amplitude of the detected signal [51, 53]. Hence, all demodulation techniques require two photodiode signals from the interferometer, usually set at a phase difference of $\pi/2$. This way, one can use the complementary properties of the two signals and enhance the dynamic range of the signal [52, 54].

The two most common techniques for phase demodulation require a fiber Mach-Zehnder interferometer with a path imbalance isolated from environmental noise and thermal drifts, and an in-line Piezoelectric Transducer (PZT). The PZT can either be used to keep the interferometer in quadrature (i.e. $\Delta\phi = 0$) using a feedback mechanism [55]; or by using a high frequency carrier for modulating the phase of the interferometer [51]. However, to build a low-noise stabilised circuit to control the PZT in either mechanism was beyond the scope of the project.

Therefore, we used the symmetric 3×3 coupler Fiber interferometer (as shown in figure 4.3) to obtain the phase demodulation, as implemented in [52]. The 3×3 coupler is a fused fiber coupler enabling us to combine three different optical signals into a single fiber (and also obtain two separate outputs that can be measured using two photo-diodes). In addition, the coupler intrinsically bears a phase difference of

$2\pi/3$ between the two outputs, hence we can take advantage of the complementary properties without including any external active components to this device.

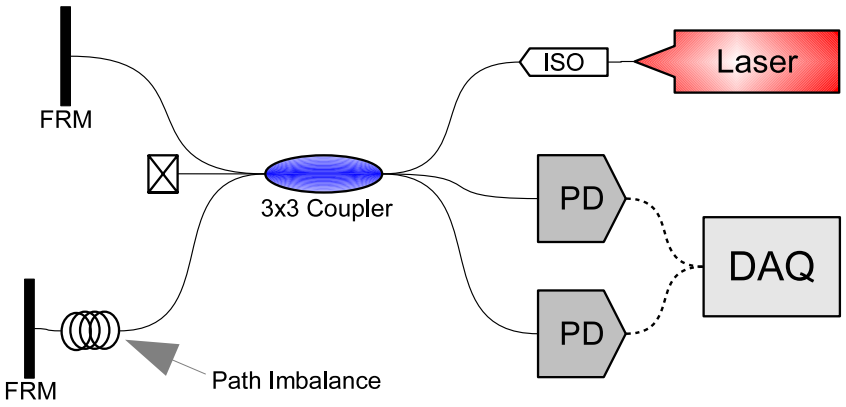

Figure 4.3: Experimental setup for Digital Phase demodulation. FRM: Faraday Rotating Mirror; ISO: Isolator; PD: Photodiode to convert the intensity of light into current. DAQ: Data Acquisition device used for Analog to Digital conversion of the signal

We set up a Michelson Interferometer using a symmetrical 3×3 coupler instead of the usual 2×2 coupler. Only two of the arms are being used, while the third is tightly bent to prevent any back reflections. An isolator (ISO) is used to deplete the interference signal before it approaches back to the laser under test, while the other two arms are connected to the photo-diodes, and are used for the phase demodulation.

The transfer matrix for the 3×3 coupler can be written as follows [56, 57]:

$$M_{3\times3} = \frac{e^{-iKl}}{3}\begin{bmatrix} 1 & 1 & 1 \\ 1 & 1 & 1 \\ 1 & 1 & 1 \end{bmatrix} + \frac{e^{iKl}}{3}\begin{bmatrix} 2 & -1 & -1 \\ -1 & 2 & -1 \\ -1 & -1 & 2 \end{bmatrix} \tag{4.4}$$

Where K is the coupling coefficient, and l is the length of the coupling section of the fiber.

On the other hand, after the light has passed through the coupler, the interferometer induces a relative phase shift $\phi_s/2$ due to the additional length L in one of the arms. The Faraday Rotating Mirror (FRM) reflects this delayed light and also rotates the polarization by 90^o, making the reflected beam independent of the actual

birefringence of the fiber [20]. Finally, neglecting the polarization effect, the net delay after the reflection can be expressed as follows [20, 56, 57]:

$$D = \begin{bmatrix} 1 & 0 & 0 \\ 0 & 0 & 0 \\ 0 & 0 & e^{i\phi_s} \end{bmatrix} \tag{4.5}$$

Representing the incident beam due to the laser field as $E_{in} = \begin{bmatrix} E_1(t) \\ 0 \\ 0 \end{bmatrix}$, the resulting field from the interferometer becomes:

$$\begin{aligned} E_{out} &= [M_{3\times3}][D][M_{3\times3}]E_{in} \\ &= \frac{E_1(t)}{9} \begin{bmatrix} (3\cos(Kl) - i\sin(Kl))^2 - 4e^{i\phi_s}\sin(Kl)^2 \\ 2i\sin(Kl)(3\cos(Kl) - i\sin(Kl)) - 4e^{i\phi_s}\sin(Kl)^2 \\ 2i\sin(Kl)(3\cos(Kl) - i\sin(Kl))(e^{i\phi_s} + 1) \end{bmatrix} \end{aligned} \tag{4.6}$$

For the ideal condition, we need $\cos(2Kl) = -1/2$, and the losses in both arms to be the same. With these conditions in mind, we obtain the laser intensities incident on the photo-diode to be:

$$\begin{aligned} I_2 &= E^*_{out,2}E_{out,2} = \frac{2}{9}I_1(1 + \cos(\phi_s - 2\pi/3)) \\ I_3 &= E^*_{out,3}E_{out,3} = \frac{2}{9}I_1(1 + \cos(\phi_s)) \end{aligned} \tag{4.7}$$

where $I_1 = E^*_1(t)E_1(t)$

However, in reality, these ideal conditions are not achieved that easily. The coupling coefficient K and the fiber loss may change with the environmental perturbation. With these factors in mind, the two outputs of the interferometer can be generally

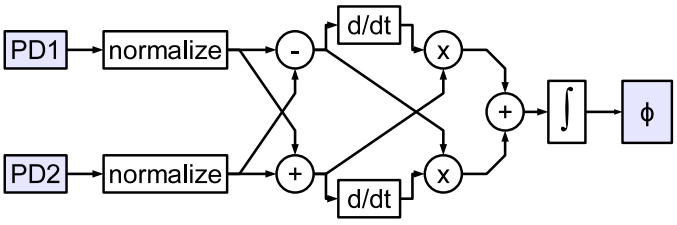

Figure 4.4: Flowchart for the DCM algorithm

written as [52]:

$$D_2 = A_1 + B_1 \cos(\phi_s - 2\pi/3) \tag{4.8}$$
$$D_3 = A_2 + B_2 \cos(\phi_s)$$

where A_1, A_2 and B_1, B_2 represent the average intensities and the contribution of the interference respectively. Ideally, the phase difference ϕ_s would be a static value. However, due to the environmental perturbations and, in this case, the frequency noise of the laser, ϕ_s becomes a time varying signal. It is this phase signal ϕ_s that is of our interest, and will be used to derive the frequency noise of our laser.

Differential-Cross Multiplication Phase Demodulation Algorithm

Once the Voltage readings D_2 and D_3 are acquired from the interferometer, they are passed through the Differential-Cross Multiplication Algorithm. First, each reading is normalized so that it ranges between 1 and -1. The values I_C and I_S (after normalizing both waveforms D_2 and D_3 into I_2 and I_3 respectively) are as follows:

$$I_C = I_2 + I_3 = -cos(\phi_s(t))$$
$$I_S = I_2 - I_3 = \sqrt{3}sin(\phi_s(t)) \tag{4.9}$$

Now, as I_C and I_S are passed through the differentiator:

$$\begin{aligned} \frac{dI_C}{dt} &= sin(\phi_s(t))\frac{d\phi_s(t)}{dt} \\ \frac{dI_S}{dt} &= \sqrt{3}cos(\phi_s(t))\frac{d\phi_s(t)}{dt} \end{aligned} \tag{4.10}$$

Lastly, cross-multiplying the differentiated values of I_C and I_S with the original values, the net result obtained is:

$$\begin{aligned} I_S\frac{dI_C}{dt} - I_C\frac{dI_S}{dt} &= \sqrt{3}sin(\phi_s(t)) \times sin(\phi_s(t))\frac{d\phi_s(t)}{dt} \\ &\quad + cos(\phi_s(t)) \times \sqrt{3}cos(\phi_s(t))\frac{d\phi_s(t)}{dt} \\ &= \sqrt{3}\frac{d\phi_s(t)}{dt}[cos(\phi_s(t))^2 + sin(\phi_s(t))^2] \end{aligned}$$

Hence,

$$I_S\frac{dI_C}{dt} - I_C\frac{dI_S}{dt} = \sqrt{3}\frac{d\phi_s(t)}{dt} \tag{4.11}$$

The time-derivative can be taken care of by dividing its Fourier transform with ω such that:

$$|\mathcal{F}\left[\phi_s(t)\right]|(\omega) = \frac{|\mathcal{F}\left[\frac{\mathrm{d}\phi_s(t)}{\mathrm{d}t}\right]|}{\omega} \tag{4.12}$$

Determining the frequency noise from the response of the interferometer

Assume there is a frequency modulated signal, where the modulation is driven at a frequency ω_m, and the modulation strength is β_m:

$$E(t) = E_0 \sin\left(\omega_0 t + \frac{\beta_m}{f_m}\cos(\omega_m t)\right) \tag{4.13}$$

Hence, in this case, the phase difference between the two arms in the interferometer can be expressed as:

$$\begin{aligned}\phi_s &= \left(\omega_0 t + \frac{\beta_m}{f_m}\cos(\omega_m t)\right) - \left(\omega_0(t-t_d) + \frac{\beta_m}{f_m}\cos(\omega_m(t-t_d))\right) \\ &= \omega_0 t_d - \frac{\beta_m}{f_m}\sin(\omega_m t_d)\sin(\omega_m(t-t_d/2))\end{aligned} \tag{4.14}$$

where $t_d = nL/c$ is the time delay imposed by a path difference of length L. Hence, temporal fluctuations in the phase difference $\phi_s(t)$ can be expressed as follows:

$$\begin{aligned}\Delta\phi_s(t) &= -\frac{\beta_m}{f_m}\sin(\omega_m t_d)\sin(\omega_m(t-t_d/2)) \\ &= -\frac{2\pi nL\beta_m}{c}\text{sinc}\left(\frac{\omega_m nL}{c}\right)\sin(\omega_m(t-t_d/2))\end{aligned} \tag{4.15}$$

Finally, by applying a Fourier transform, we see that the spectral density of the phase difference S_{ϕ_s} is simply:

$$S_{\phi_s}(\omega) = \left[\frac{2\pi nL\beta_m}{c}\text{sinc}\left(\frac{\omega_m nL}{c}\right)\right]^2 \delta(\omega-\omega_m) \tag{4.16}$$

Using this analogy, we can hence claim that the phase noise $S_{\phi_s}(\omega)$ derived from the interferometer is related to the frequency noise $S_\nu(\omega)$ of a given laser as follows:

$$S_{\phi_s}(\omega) = \left[\frac{2\pi nL}{c}\text{sinc}\left(\frac{\omega nL}{c}\right)\right]^2 S_\nu(\omega) \tag{4.17}$$

When $\omega nL/c \ll 1$, then $\text{sinc}\left(\frac{\omega nL}{c}\right) \sim 1$, resulting in the following linear equation:

$$S_{\phi_s}(\omega) = \left[\frac{2\pi nL}{c}\right]^2 S_\nu(\omega) \tag{4.18}$$

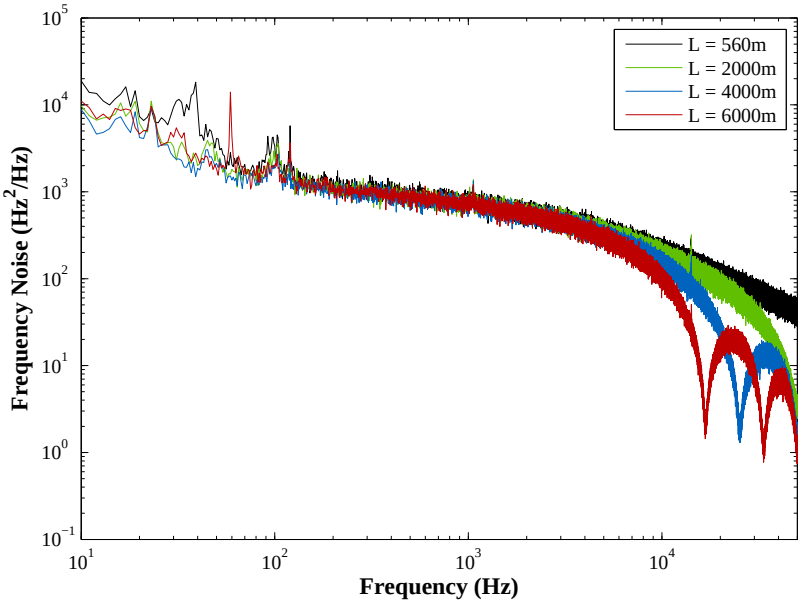

Figure 4.5: Frequency Noise Measurements for standard EDF laser using different path delays (L) in the 3×3 coupler phase demodulator.

Frequency Noise for a Commercial Laser using Variable Interferometer Path Delays

The frequency noise measurement was tested using a standard EDF fiber laser as it attains a broad frequency noise profile spanning beyond 100kHz. The effect of the sinc roll-off for different interferometric path delays is clearly visible as shown in figure 4.5. We realize that as long as we don't extend the path delays beyond 6km, the sinc roll-off can be neglected for frequencies less than 10kHz. Nevertheless, provided we stay within the limits imposed by the sinc function, we should be able to obtain a stable result for the frequency noise for our lasers. Also, we realize that we would need to use multiple path lengths in our interferometer just to verify the contribution of the noise.

4.3 Relative Intensity Noise Measurements

The Relative intensity noise describes the fluctuations in the intensity of a given laser. It can be expressed as follows:

$$RIN = \frac{\langle \Delta I(t) \Delta I(t-\tau) \rangle}{I_0^2} \rangle \tag{4.19}$$

where $\Delta I(t)$ is the temporal fluctuations in the intensity, while I_0 is the average intensity of the laser. The statistical features of this noise can then be described using the spectral density of the RIN, which is simply the Fourier transform of the autocorrelation shown above.

The measurement for the RIN were simply done by measuring the intensity of light emitted by the lasers using the Thorlabs PD130C photo-detector. Time traces of the signal for each laser were stored, after which we applied the Fast Fourier Transform to determine the power spectral density of the Relative Intensity Noise. This Power Spectral density was normalized with respect to the average power of the signal. Although we could have implemented more rigorous schemes to reduce the contribution of the ground noise from the photo-detector as shown in [58], we instead relied on a qualitative comparison with respect to other commercially available low-noise lasers with electronic feedback mechanisms.

Chapter 5

Results and Discussions

5.1 Frequency Noise Measurements

Frequency and intensity noise measurements were conducted for the following lasers:

- EDF random laser with 560 m, 1000 m and 25,000 m Rayleigh scattering optical fiber.
- BRFL with a 10km fiber used for both the Brillouin gain and Rayleigh feedback.
- Non-Planar Ring Oscillator (NPRO), which is considered a benchmark for narrow linewidth laser (Lightwave Electronics, Nd:YAG. This laser was not used for Intensity Noise measurements.
- Standard fiber laser consisting of a composite of active (EDF) and passive fiber (NP-Photonics, 3kHz linewidth).

The last two are commercially available low-noise lasers, and will be used for comparison purposes in this chapter. For frequency noise measurements, the first three lasers were introduced to a path imbalance of 4000m in the 3×3 phase demodulator, while the last laser had an imbalance of 560m.

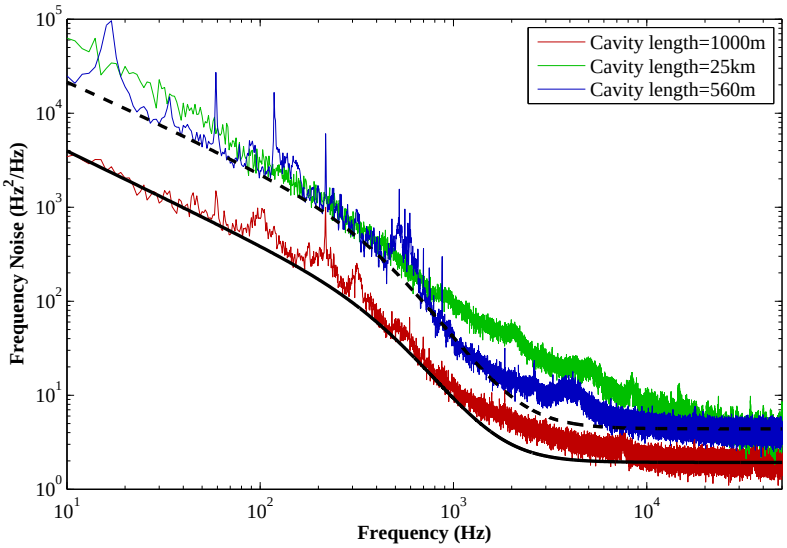

Figure 5.1: Frequency Noise for EDF Random lasers with different Rayleigh fiber lengths. The black curves represent the parameter fitting for the corresponding random laser. Parameter values for the theoretical curves are shown in Table 5.1

5.2 Frequency Noise Results for EDF Random lasers

Figure 5.1 and table 5.1 show that our theory for EDF random lasers (chapter 3) is in good agreement with the experimental results for the 560 m and 1000 m random lasers. Since the gain fiber is of the same length in both cases, contributions from the non-equilibrium thermal noise S_{neq} remain the same. However, since the thermal noise is inversely proportional to the effective cavity length, the equilibrium thermal noise S_{eq} should decrease with increasing fiber length. This is evident from the results as the frequency noise is reduced by almost a half when the length is almost doubled (560 m $\rightarrow$ 1000 m). From table 5.1, we can also see a consistency in the linewidth represented by the Lorentzian envelope, as it does not vary significantly with fiber length, and depends only on the intrinsic nature of the laser components. Lastly, at higher frequency, we reach ground noise levels (defined by parameter B in table 5.1) which arise from the instability of the apparatus in a noisy environment. We can definitely state this ground noise is not arising from the laser, as that would result in the presence of a sinc roll-off in the 20kHz mark for a 4000 m imbalance in the phase demodulator (figure 4.5).

This model, however, fails as we further increase the length of the scattering

Table 5.1: Parameter values for Frequency Noise curves in Figure (5.1)

Cavity Length	1000m	560m
A (Hz^3/Hz)	47.37	229.06
B (Hz^2/Hz)	1.93	4.3917
Linewidth $\left(\frac{\alpha\nu}{2\pi}\right)$ (Hz)	872.8	865.8

fiber to 25 km. The impact of the Lorentzian envelope begins to diminish, and the thermal noise almost appears to bear the characteristics $1/f$ curve once again. For this situation, we can argue that additional unwanted nonlinear optical processes begin to infiltrate the system, something that the model does not take into account. We realise that for long lengths (25km), the threshold for Spontaneous Brillouin scattering is greatly lowered to about 2-3mW [59]. This results in additional density fluctuations from electrostriction, and introduces additional frequency noise characteristics that supplement the already existing thermal frequency noise.

Comparison between the 1000 m EDF random laser and other narrow-linewidth lasers has been shown in Fig. 5.2. NPRO lasers are known to exhibit the characteristic $1/f$ noise for frequencies less than than 10kHz [41]. The EDF fiber laser initially exhibits a $1/f$ noise at frequencies below 100 Hz contributed by S_{neq}, followed by a roll-off at frequencies above 10kHz from S_{eq}, as predicted by the thermal noise characteristics for standard fiber lasers (chapter 3). The random laser, on the other hand, when compared to the standard fiber laser, clearly shows a significant suppression of the thermal noise due to the Rayleigh feedback, providing a steeper roll-off beginning at 1kHz. The random laser, EDF fiber laser, and the NPRO laser exhibit a noise level of 6 Hz^2/Hz, 1000 Hz^2/Hz and 15 Hz^2/Hz respectively at 2 kHz, showing us that a free-running random laser can achieve noise levels that are even lower than commercially available benchmark narrow-linewidth lasers in the 1-10 kHz range.

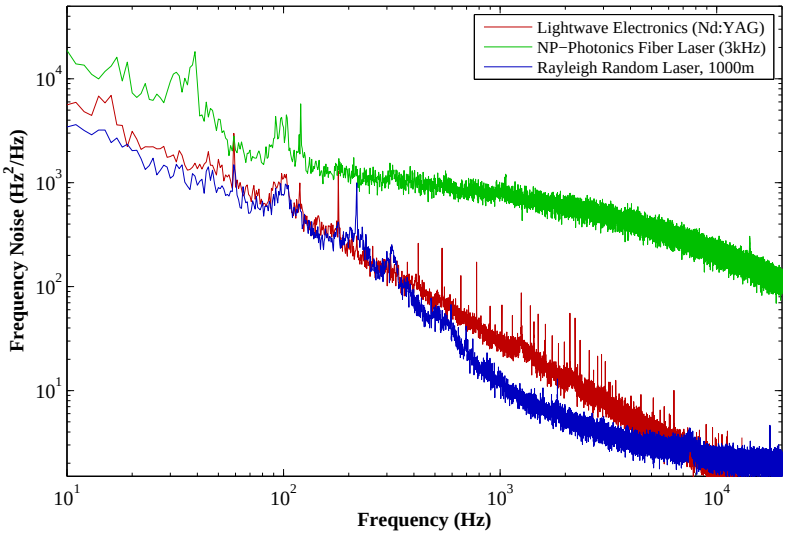

Figure 5.2: Frequency Noise Spectral Density of the Random Laser (1000m) compared with EDF fiber laser and NPRO laser

5.3 Relative Intensity Noise Results

RIN measurements for the three EDF random lasers, BRFL and EDF fiber laser (NP-Photonics) are shown in figure 5.3. The EDF fiber laser, being a commercial laser, includes special RIN suppression techniques using an electronic feedback circuit, and hence acts as a benchmark for all the other random lasers. At present, within the 100 kHz range, the noise levels for the free running random lasers exceed that of the EDF fiber laser by about 4 to 5 orders of magnitude.

For the case of EDF random lasers, the 560 m and 1 km random lasers show a series of similar peaks around the 100-200 Hz range which occur due to intrinsic noise from the EDF, as well as the pump laser. Moreover, because the random laser lacks any feedback mechanisms for longitudinal mode stability, any sudden mode-hopping in the laser is responded by damped oscillation due to the long relaxation time of the gain media (∼8-10 ms [20]). This phenomena explains the distinct peaks in the 5-10 kHz range for all three random lasers. However, in contrast to EDF-related noise characteristics, there is also the incomplete suppression of the 'continuous' mode distribution, resulting in high noise values found in the low frequency range. Because of the large Rayleigh fiber length, the laser intrinsically exhibits an extremely dense

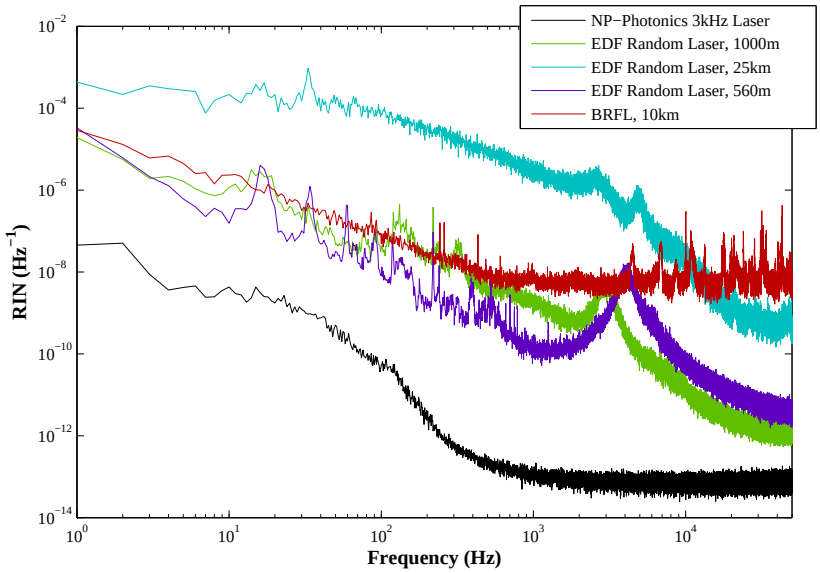

Figure 5.3: Relative Intensity Noise for EDF Random lasers, BRFL and EDF fiber laser (NP-Photonics)

mode structure which is almost impossible to suppress with an inadequately broad filter ($\sim$ 3 GHz for FBG). Moreover, this effect gets worse as the fiber length is increased due to larger accumulation of the Rayleigh feedback and a higher density in the mode distribution. This is clearly visible for the 25 km random laser as this noise dominates over the intrinsic EDF noise that is apparent in the 560m and 1000m lasers.

In the case of the BRFL, the laser exhibits randomly distributed discrete peaks in the high frequency range ($>$ 1 kHz). These peaks mainly arise because of the random mode hopping between two distinct modes in the random laser, which can only be possible in the presence of high mode selectivity for the Brillouin gain. In contrast to the stimulated emission in the EDF gain medium is a process that requires strong matching conditions for the phase and polarization between the Stokes and pump wave. Therefore, this process depletes the continuous mode distribution imposed by the Rayleigh fibers, and only allows a distinct set of modes to take part in lasing. Furthermore, this discrete gain profile for the BRFL, which is derived from the optical fiber itself, is also prone to thermal fluctuations. Essentially, the discrete gain profile for the Stokes wave can be represented as follows:

$$G(\Omega) = \sum_i \frac{G_i}{1 + 4\dfrac{(\Omega - \Omega_{\beta i})^2}{\Gamma_{\beta i}}} \tag{5.1}$$

where $\Omega = \omega - \omega_p$ is the frequency shift from the pump laser, G_i is the maximum gain provided to each mode, and $\Gamma_{\beta i}/2$, which is typically in the order 10 MHz, represents the linewidth of the Lorentzian gain profile centred at $\Omega_{\beta i}$ away from the pump frequency. This linewidth arises due to relaxation oscillation of the acoustic waves, which is typically < 10 ns in optical fibers [19]. Each beat frequency $\Omega_{\beta i}$ is expressed as:

$$\Omega_{\beta i} = \frac{4\pi n_p \nu_A}{\lambda_p} \tag{5.2}$$

Where ν_A is the speed of sound in the fiber ($= 5.96$ km s^{-1}) and $n_p = 1.45$ is the effective mode index at pump wavelength λ_p [19]. If we assume n_p mainly to be dependent on temperature, then it is clear that thermal fluctuations in the fiber will drift each of the Lorentzian gain profiles away from their resonant frequencies $\Omega_{\beta i}$. Typical gain frequency shift is in the order of $\sim$ 10 kHz for a temperature shift of $\sim 0.01^oC$ [19], which may seem negligibly small when compared to a MHz-wide spectrum, but becomes a crucial matter for the mode stability when a selected Brillouin gain profile narrows down during lasing conditions.

5.4 Frequency noise of Random Laser by EDF and Brillouin gain

Comparison between the 1000 m EDF random laser and BRFL are show in figure 5.4. From this result, as well as our discussion in section 5.3, we hypothesize the following points:

- We realize that both lasers impose suppression of frequency noise in the high frequency range. In the case of the EDF laser, we hypothesized that this was mainly because of a large section of passive Rayleigh scattering fiber that provides a Lorentzian envelope to the $1/f$ noise from the active EDF (chapter 3). We can argue the same for the BRFL, and suggest that most of the Brillouin gain is mainly provided by a relatively short section of the 10 km fiber. The rest of the fiber aids in the accumulation of the Stokes wave through Rayleigh Scattering, resulting in a pseudo-Lorentzian envelope over the intrinsic frequency noise.

- In addition to the thermal noise arising from the passive fiber (S_{eq}), an additional noise source originates due to the acoustic fluctuations from the active Brillouin fiber section. The statistics for these fluctuations will be governed by the acoustic wave equation (equation 3.44, and hence may contribute differently and not obey the characteristic $1/f$ trend as seen for the EDF laser.

- The gain from the EDF fiber is stable, and is evenly distributed to support the amplification of all the possible modes that are present due to the Rayleigh fiber. Hence, any deviations from the nominal frequency during lasing are only to arise due to the density fluctuations in the fiber. On the other hand, as mentioned in section 5.3, the gain spectrum for the Brillouin laser is discrete and can only favour amplification for a specific number of modes. Furthermore, from equation 5.2, we see that the central frequency for each Lorentzian gain profile depends on the thermally fluctuating refractive index of the pump wavelength, forcing the gain to slowly drift from its nominal peak. Hence, this additional noise from the Brillouin gain is bound to contribute towards the frequency noise for this laser.

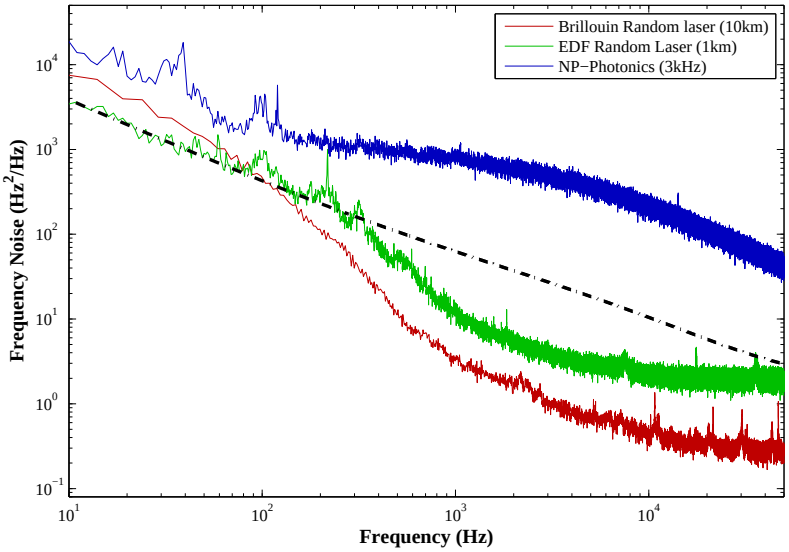

Figure 5.4: Frequency Noise Spectral Density of the EDF Random Laser (1000m), EDF fiber laser and BRFL. Dotted curve represents the $1/f$ noise for a 1000m EDF laser with no Rayleigh feedback

Chapter 6

Conclusion

We have fully characterized the frequency and intensity noise for a novel EDF random laser with an ultra-long Rayleigh feedback fibers. We find that by using a 1.3 m EDF, a 1 km Rayleigh scattering fiber, and a FBG, frequency noise levels outshine commercially available narrow-linewidth lasers which include external feedback mechanisms for frequency and intensity noise suppression. A theoretical model for the frequency noise of these random lasers agrees well with experimental results, as demonstrated for the 560 m and 1 km random lasers. Through this model, we conclude that EDF random lasers have the ability to suppress the intrinsic thermal frequency noise from cavity fiber lasers due to the Lorentzian envelope attributed by the Rayleigh scattering in ultra-long fibers.

We have also demonstrated a novel Brillouin random laser by simply using a bi-directionally pumped 10 km fiber. Although no analytical solutions for the frequency noise have been acquired till date, a preliminary approach towards the derivation has been speculated. This proposed model will take into account the supplementing acoustic fluctuations within the fiber, whose statistics will depend on the acoustic wave equation. It has also been shown through RIN measurements that such lasers do not acquire a 'continuous' mode distribution as found in EDF lasers, and only consist of a discrete set of modes due to the selective Brillouin gain.

Future work could look into optimizing the lasers by trying to shorten the cavity length even further, and yet still maintain the same lasing threshold and power

efficiency. We also hope that the results shown in this thesis spark interest in the fiber community, and eventually lead to a better model that is able to characterize the noise for a random laser with any distributive gain profile, and takes into account both the thermal and acoustic fluctuations present in the fiber. With further emphasis on frequency and intensity stabilization techniques, this new class of low frequency noise lasers show potential in surpassing the limitations of commercially available narrow-linewidth lasers, and can probably be applied in various fields such as metrology and interferometer based sensing applications.

Chapter 7

Bibliography

[1] Emmanuel Desurvire and Jay R Simpson. Amplification of spontaneous emission in erbium-doped single-mode fibers. *Lightwave Technology, Journal of*, 7(5):835–845, 1989.

[2] Sajeev John. Electromagnetic absorption in a disordered medium near a photon mobility edge. *Phys. Rev. Lett.*, 53:2169–2172, Nov 1984.

[3] Diederik S. Wiersma. The physics and applications of random lasers. *Nature Physics*, 4:359 – 367, May 2008.

[4] E. Abrahams, P. W. Anderson, D. C. Licciardello, and T. V. Ramakrishnan. Scaling theory of localization: Absence of quantum diffusion in two dimensions. *Phys. Rev. Lett.*, 42:673–676, Mar 1979.

[5] RV Ambartsumyan, NG Basov, PG Kryukov, and VS Letokhov. Non-resonant feedback in lasers. *Progress in Quantum Electronics*, 1:107, 1970.

[6] Zolin V. F. Markushev, V .M. and Ch. M. Briskina. Power laser. *Zh. Prikl. Spektrosk.*, 45:847–850, 1986.

[7] C Gouedard, D Husson, C Sauteret, F Auzel, and A Migus. Generation of spatially incoherent short pulses in laser-pumped neodymium stoichiometric crystals and powders. *JOSA B*, 10(12):2358–2363, 1993.

[8] Jordi Martorell, RM Balachandran, and NM Lawandy. Radiative coupling between photonic paint layers. *Optics letters*, 21(4):239–241, 1996.

[9] C. W. J. Beenakker. Thermal radiation and amplified spontaneous emission from a random medium. *Phys. Rev. Lett.*, 81:1829–1832, Aug 1998.

[10] Lucia Florescu and Sajeev John. Photon statistics and coherence in light emission from a random laser. *Phys. Rev. Lett.*, 93:013602, Jul 2004.

[11] H. Cao, Y. Ling, J. Y. Xu, C. Q. Cao, and Prem Kumar. Photon statistics of random lasers with resonant feedback. *Phys. Rev. Lett.*, 86:4524–4527, May 2001.

[12] V. M. Apalkov, M. E. Raikh, and B. Shapiro. Random resonators and prelocalized modes in disordered dielectric films. *Phys. Rev. Lett.*, 89:016802, Jun 2002.

[13] A. A. Chabanov, Z. Q. Zhang, and A. Z. Genack. Breakdown of diffusion in dynamics of extended waves in mesoscopic media. *Phys. Rev. Lett.*, 90:203903, May 2003.

[14] Sushil Mujumdar, Marilena Ricci, Renato Torre, and Diederik S. Wiersma. Amplified extended modes in random lasers. *Phys. Rev. Lett.*, 93:053903, Jul 2004.

[15] Sergei K Turitsyn, Sergey A Babin, Atalla E El-Taher, Paul Harper, Dmitriy V Churkin, Sergey I Kablukov, Juan Diego Ania-Castañón, Vassilis Karalekas, and Evgenii V Podivilov. Random distributed feedback fibre laser. *Nature Photonics*, 4(4):231–235, 2010.

[16] Stefano Gottardo, Stefano Cavalieri, Oleg Yaroshchuk, and Diederik S. Wiersma. Quasi-two-dimensional diffusive random laser action. *Phys. Rev. Lett.*, 93:263901, Dec 2004.

[17] Andrei A. Fotiadi. Random lasers: An incoherent fibre laser. *Nature Photonics*, 4:204 – 205, 2010.

[18] Xiaoyi Bao and Liang Chen. Recent progress in distributed fiber optic sensors. *Sensors*, 12(7):8601–8639, 2012.

[19] G. P. Agrawal. *Nonlinear Fiber Optics.* Elsevier LTD., 2007.

[20] Rongqing Hui and Maurice O'Sullivan. *Fiber Optic Measurement Techniques.* Academic Press, 2008.

[21] Robert W Boyd. *Nonlinear Optics. Third Edition.* Academic press, 2010.

[22] AE El-Taher, Mercedes Alcon-Camas, SA Babin, Paul Harper, Juan Diego Ania-Castañón, and Sergei K Turitsyn. Dual-wavelength, ultralong raman laser with rayleigh-scattering feedback. *Optics letters*, 35(7):1100–1102, 2010.

[23] DV Churkin, SA Babin, AE El-Taher, Paul Harper, SI Kablukov, Vasileios Karalekas, Juan Diego Ania-Castañón, EV Podivilov, and SK Turitsyn. Raman fiber lasers with a random distributed feedback based on rayleigh scattering. *Physical Review A*, 82(3):033828, 2010.

[24] SA Babin, AE El-Taher, P Harper, EV Podivilov, and SK Turitsyn. Tunable random fiber laser. *Physical Review A*, 84(2):021805, 2011.

[25] Ilya D Vatnik, Dmitriy V Churkin, Sergey A Babin, and Sergei K Turitsyn. Cascaded random distributed feedback raman fiber laser operating at 1.2 μm. *Optics express*, 19(19):18486–18494, 2011.

[26] Wei Li Zhang, Yun Jiang Rao, Jun Mei Zhu, Zi Xin Yang Zi Nan Wang, and Xin Hong Jia. Low threshold 2nd-order random lasing of a fiber laser with a half-opened cavity. *Optics express*, 20(13):14400–14405, 2012.

[27] Meng Pang, Xiaoyi Bao, and Liang Chen. Observation of narrow linewidth spikes in the coherent brillouin random fiber laser. *Opt. Lett.*, 38(11):1866–1868, Jun 2013.

[28] Meng Pang, Xiaoyi Bao, Liang Chen, Zengguang Qin, Yang Lu, and Ping Lu. Frequency stabilized coherent brillouin random fiber laser: theory and experiments. *Opt. Express*, 21(22):27155–27168, Nov 2013.

[29] N Lizárraga, NP Puente, EI Chaikina, TA Leskova, and ER Méndez. Single-mode er-doped fiber random laser with distributed bragg grating feedback. *Optics express*, 17(2):395–404, 2009.

[30] Mathieu Gagné and Raman Kashyap. Demonstration of a 3 mw threshold er-doped random fiber laser based on a unique fiber bragg grating. *Optics express*, 17(21):19067–19074, 2009.

[31] Tao Zhu, Xiaoyi Bao, and Liang Chen. A single longitudinal-mode tunable fiber ring laser based on stimulated rayleigh scattering in a nonuniform optical fiber. *Lightwave Technology, Journal of*, 29(12):1802–1807, June 2011.

[32] Guolu Yin, Bhavaye Saxena, and Xiaoyi Bao. Tunable er-doped fiber ring laser with single longitudinal mode operation based on rayleigh backscattering in single mode fiber. *Opt. Express*, 19:25981–25989, 2011.

[33] Tao Zhu, Xiaoyi Bao, Liang Chen, Hao Liang, and Yongkang Dong. Experimental study on stimulated rayleigh scattering in optical fibers. *Opt. Express*, 18:22958–22963, 2010.

[34] Rudiger Paschotta. Encyclopedia of laser physics and technology. *http://www.rp-photonics.com/encyclopedia.html. Accessed on 8 July, 2014*, December 2001.

[35] Bornain Chiu and Mardi C. Hastings. Characterization of frequency and phase noise. *International Radio Consultative Committee (C.C.I.R.)*, (Report 580):142–150, 1994.

[36] Susan M. Lea. *Mathematics for Physicists*. Nelson Education, 2004.

[37] Dennis Derickson. *Fiber Optic Test and Measurement*. Upper Saddle River, NJ : Prentice Hall PTR, 1998.

[38] Scott Foster, Geoffrey A. Cranch, and Alexei Tikhomirov. Experimental evidence for the thermal origin of $1/f$ frequency noise in erbium-doped fiber lasers. *Phys. Rev. A*, 79:053802, May 2009.

[39] Amnon Yariv. *Optical Electronics in Modern Communications*. Oxford University Press, USA, 1997.

[40] A. L. Schawlow and C. H. Townes. Infrared and optical masers. *Phys. Rev.*, 112:1940–1949, Dec 1958.

[41] G. A. Cranch and G. A. Miller. Fundamental frequency noise properties of extended cavity erbium fiber lasers. *Opt. Lett.*, 36:906–908, 2011.

[42] Scott Foster. Fundamental limits on $1/f$ frequency noise in rare-earth-metal-doped fiber lasers due to spontaneous emission. *Phys. Rev. A*, 78:013820, Jul 2008.

[43] S. Foster, A Tikhomirov, and M. Milnes. Fundamental thermal noise in distributed feedback fiber lasers. *Quantum Electronics, IEEE Journal of*, 43(5):378–384, May 2007.

[44] Bhavaye Saxena, Xiaoyi Bao, and Liang Chen. Suppression of thermal frequency noise in erbium-doped fiber random lasers. *Opt. Lett.*, 39(4):1038–1041, Feb 2014.

[45] T Yoshino. Simple theoretical approach for spectral properties of rayleigh backscattering feedback fibre lasers. *Electronics letters*, 47(18):1040–1042, 2011.

[46] N Nakagawa, EK Gustafson, Peter T Beyersdorf, and MM Fejer. Estimating the off resonance thermal noise in mirrors, fabry-perot interferometers, and delay lines: The half infinite mirror with uniform loss. *Physical Review D*, 65(8):082002, 2002.

[47] H. E. Rowe. *Signals and Noise in Communication Systems*. D. Van Nostrand Company, Princeton, NJ, 1965.

[48] P. Gallion and G. Debarge. Quantum phase noise and field correlation in single frequency semiconductor laser systems. *Quantum Electronics, IEEE Journal of*, 20(4):343 – 349, apr 1984.

[49] L.B. Mercer. 1/f frequency noise effects on self-heterodyne linewidth measurements. *Lightwave Technology, Journal of*, 9(4):485 –493, apr 1991.

[50] G. M. Stéphan, T. T. Tam, S. Blin, P. Besnard, and M. Têtu. Laser line shape and spectral density of frequency noise. *Phys. Rev. A*, 71:043809, Apr 2005.

[51] A. Dandridge, A. Tveten, and T. Giallorenzi. Homodyne demodulation scheme for fiber optic sensors using phase generated carrier. *IEEE Journal of Quantum Electronics*, 18(10):1647 – 1653, oct 1982.

[52] M. Pang, M. Zhang, L. W. Wang, W. Jin, and Y. B. Liao. A digital passive phase demodulation scheme using 3 x 3 coupler for fiber-optic interferometric sensors. volume 7004, page 70042L. SPIE, 2008.

[53] Bornain Chiu and Mardi C. Hastings. Digital demodulation for passive homodyne optical fiber interferometry based on a 3 x 3 coupler. *Proc. SPIE*, 2292:371 – 382, 1994.

[54] Clay K Kirkendall and Anthony Dandridge. Overview of high performance fibre-optic sensing. *Journal of Physics D: Applied Physics*, 37(18):R197, 2004.

[55] Bartolo RE, Tveten A, Kirkendall CK, Juodawlkis PW, Loh W, and Plant JJ. Characterization of a low-phase-noise, high-power (370 mw), external-cavity semiconductor laser. *Naval Research Laboratory, Washington DC*, 2010.

[56] Youxin Mao, Costel Flueraru, Sherif Sherif, and Shoude Chang. 3 x 3 mzi with unbalanced differential detection for full range swept-source optical coherence tomography. volume 7099, page 709909. SPIE, 2008.

[57] S.K. Sheem. Optical fiber interferometers with 3 x 3 directional couplers: Analysis. *Journal of Applied Physics*, 52(6):3865 – 3872, jun. 1981.

[58] E. Rubiola, K. Volyanskiy, and L. Larger. Measurement of the laser relative intensity noise. In *Frequency Control Symposium, 2009 Joint with the 22nd European Frequency and Time forum. IEEE International*, pages 50–53, April 2009.

[59] Valeri I Kovalev and Robert G Harrison. Threshold for stimulated brillouin scattering in optical fiber. *Optics express*, 15(26):17625–17630, 2007.